

Distributional Active Inference

Abdullah Akgül¹ Gulcin Baykal¹ Manuel Haußmann¹ Mustafa Mert Çelikok¹ Melih Kandemir¹

Abstract

Optimal control of complex environments with robotic systems faces two complementary and intertwined challenges: efficient organization of sensory state information and far-sighted action planning. Because the reinforcement learning framework addresses only the latter, it tends to deliver sample-inefficient solutions. Active inference is the state-of-the-art process theory that explains how biological brains handle this dual problem. However, its applications to artificial intelligence have thus far been limited to extensions of existing model-based approaches. We present a formal abstraction of reinforcement learning algorithms that spans model-based, distributional, and model-free approaches. This abstraction seamlessly integrates active inference into the distributional reinforcement learning framework, making its performance advantages accessible without transition dynamics modeling.

1. Introduction

The human brain is an experience machine (Clark, 2024): a survival system that enables far-sighted planning by efficiently organizing complex multimodal sensory input. As the most advanced general intelligence we know, it is a natural inspiration for autonomous agents. Yet it remains unclear how the brain structures sensory stimuli into decision-relevant variables to solve control and adaptation problems so efficiently (Dorrell et al., 2023). Reinforcement learning (RL) formalizes far-sighted planning, and recent advances enable web-scale learning of multimodal distributions for general-purpose action generation (Kim et al., 2024; Black et al., 2024; NVIDIA Research et al., 2025). Still, we lack a satisfying account of how such rich representations are organized for efficient planning under tight computational and data constraints (Botteghi et al., 2025).

The *active inference framework* (AIF) offers a process-level

theory of whole-brain information organization (Friston et al., 2017; Parr et al., 2022). It posits an action–perception cycle in which neural dynamics for perception and control evolve to minimize a single objective, the expected free energy (EFE) (Friston et al., 2015). Formally, this amounts to variational Bayes on a controlled Markov process, yielding a form of model-predictive control. Its links to modern machine learning have motivated AIF-inspired adaptive control methods (Millidge et al., 2020; Tschantz et al., 2020b; Millidge, 2021; Lanillos et al., 2021; Schneider et al., 2022; Malekzadeh & Plataniotis, 2024), but in practice these efforts have largely rederived familiar information-theoretic exploration heuristics (e.g., information gain) (Houthooft et al., 2016; Sukhija et al., 2025). To date, AIF has not delivered major practical gains in state-of-the-art RL.

Observing that the brain is an efficient information-processing system, we investigate whether AIF is useful in situations where high-fidelity forward simulation is infeasible. As *distributional RL* (Bellemare et al., 2017; 2023) provides a computationally efficient alternative to model-based RL, we aim to incorporate AIF into this framework. We achieve this goal in three steps. Firstly, we analyze AIF strictly through the lens of variational Bayesian and causal inference, reconstructing its formulation by applying a mechanistic deduction chain over a coherent set of formal entities. By expressing the prior construction via do-calculus (Pearl, 1995), we show that the standard objective admits a simpler equivalent of its commonly adopted form.

Secondly, we formalize a new theoretical framework, called *push-forward RL*, that explains the return distribution as pushing the trajectory measure of a specific policy-induced state transition kernel forward with a return functional. This recipe enables us to relate Bellman updates to the transition kernels implied by the resulting push-forwards of trajectory measures, thereby connecting model-based and model-free views of policy iteration. We use this connection to embed active inference into the distributional RL framework.

Lastly, we exploit our theoretical findings to curate a general-purpose policy optimization algorithm called *Distributional Active Inference* (DAIF). DAIF proves to be an intuitive and easily implementable extension of distributional RL. Specifically, DAIF performs temporal-difference quantile matching on a probabilistic embedding space constructed by a state-action amortized parametric distribution. Across

¹Department of Mathematics and Computer Science, University of Southern Denmark. Correspondence to: Melih Kandemir <kandemir@imada.sdu.dk>.

a broad suite of tabular and continuous-control tasks, we find that this simple modification delivers substantial performance gains. The results support our view that AIF is particularly powerful when the agent has limited computational capabilities, mirroring the conditions of the biological brains it is intended to explain.

Notation. We denote probability measures by P , and by $\mathcal{P}_{\mathcal{X}}$ the set of all probability measures on the measurable space $(\mathcal{X}, \sigma(\mathcal{X}))$ for a sigma-algebra $\sigma(\mathcal{X})$. Marginalization of an intermediate random variable and conditioning on a point observation z are denoted as $P_{X|Y}P_{Y|z} \triangleq \int P_{X|Y}(\cdot|Y)P_{Y|z}(dY|z) = P_{X|z}$. For brevity, we suppress the conditioning on variables that are integrated out, e.g., $P_X P_Y$ instead of $P_{X|Y} P_Y$. By F_P and f_P we denote the cumulative distribution function and probability density function of probability measure P , respectively. See Table 2 in the appendix for the details of our notational conventions.

Problem Statement. We consider controlled Markov processes defined by a transition kernel $P(X'|X, A)$ where $X, X' \in \mathcal{X}$ denote the current and next environment states, respectively, and $A \in \mathcal{A}$ indicates the action taken by the agent at the current time step. The agent operates in a controlled Markov process with an unknown transition kernel P_* . The agent has a reward function $R : \mathcal{X} \times \mathcal{A} \rightarrow [0, R_{\max}]$, a *world model* $P_W(X, S)$ accompanied by auxiliary variables S in a latent embedding space \mathcal{S} , and a policy $\pi : \mathcal{X} \rightarrow \mathcal{A}$. The agent seeks to maximize its adaptation to the environment by updating P_W and π through its interactions with the environment which evolves according to P_* . The agent updates its policy π by estimating the discounted sum of rewards, called the *return functional*, after taking action a_0 in state x_0 and subsequently following a fixed policy π : $\mathbf{G}_{x_0, a_0}^{\pi}(\omega) \triangleq R(x_0, a_0) + \sum_{t=1}^{\infty} \gamma^t R(x_t, \pi(x_t))$ for some discount factor $\gamma \in (0, 1)$ and a trajectory of future states $\omega \triangleq (x_1, x_2, \dots) \in \mathcal{X}^{\mathbb{N}^+}$.

2. A Rigorous Formulation of Active Inference

Active inference has substantial empirical support as a meta-level process theory for cognitive neuroscience (Hodson et al., 2024). However, its algorithmic details and probability-theoretic implications allow diverse interpretations. We will next derive the AIF training objective from the first principles of Bayesian and causal inference. The outcome yields important simplifications, which paves the way for the integration of AIF into distributional RL.

Let $P_W(X, Y, S) \triangleq P_D(X|Y, S)P_0(Y, S)$ be the agent’s world model with a prior belief over the latent embeddings $P_0(Y, S)$ and a decoding likelihood $P_D(X|Y, S)$. Variable Y represents actions and variable S represents perceptions. The Evidence Lower Bound (ELBO) functional for observation x and approximate posterior $P_Q(Y, S)$ follows from

the standard machinery of variational inference

$$L(x, P_W, P_Q) = \mathbb{E}_{y, s \sim P_Q} \left[\log \left(P_D(x|y, s)P_0(y, s)/P_Q(y, s) \right) \right].$$

Maximizing this functional with respect to Q minimizes the Kullback-Leibler divergence $\text{KL}(P_Q(Y, S)||P(Y, S|x))$, as this quantity equals the Jensen gap between $\log P(X)$ and $L(x, P_W, P_Q)$. AIF is defined as an extension of variational inference to control problems in which the transition kernel and the policy are jointly optimized with the same ELBO. AIF aims to solve $P_Q := \arg \max_{P_Q} L(x, P_W, P_Q)$ with

$$f_{P_0}(Y := y) \propto \exp(\mathbb{E}_{x' \sim P_W | \text{do}(Y \sim \delta_y, S \sim P_Q)} [L(x', P_W | \text{do}(Y \sim \delta_y, S \sim P_Q), P_Q)])$$

where the $\text{do}(X \sim P_{\text{new}})$ operator denotes a *stochastic intervention* (Pearl, 1995; Eberhardt & Scheines, 2007) to the causal graph of P_W such that the distribution of variable X is replaced by P_{new} . The intervention $\text{do}(S \sim P_Q)$ is intended to incorporate the effect of past observations on future predictions. A model equipped with such a prior would favor a world model whose predicted observations best fit it. This principle is known in cognitive neuroscience as *predictive coding* (Rao & Ballard, 1999; Friston, 2009).

AIF implements a particular way of predictive coding by intervening into the world model used in the ELBO with a *desired state distribution* $P_R(X)$, which plays the role of the reward function in RL. The canonical AIF prior construction applies the product rule over the approximate world model in the reverse direction

$$\begin{aligned} P_{W | \text{do}(Y, S \sim P_Q)}(X, Y, S) &= P_D(X|Y, S)P_Q(Y, S) \\ &= \tilde{P}(Y, S|X)\tilde{P}(X) \end{aligned}$$

which yields an approximate posterior $\tilde{P}(Y, S|X)$ and the corresponding prior $\tilde{P}(X)$. The prior $\tilde{P}(X)$ is then intervened by P_R . We now point to an overlooked matter in the AIF literature. Due to the equality imposed by the product rule, the intervention on X yields (see Section A.4):

$$\begin{aligned} P_{\tilde{W}}(X, Y, S) &\triangleq \\ P_{W | \text{do}(Y, S \sim P_Q, X \sim P_R)}(X, Y, S) &= P_Q(Y, S)P_R(X) \end{aligned} \tag{1}$$

and disconnects the observable X from the latents (Y, S) . The key consequence is that the intervened distribution of (Y, S) becomes independent from X , eliminating the effort discussed in prior work about the inference of $\tilde{P}(Y, S|X)$ (Da Costa et al., 2020). Substituting this outcome into the prior construction developed above, we obtain

$$f_{P_0}(Y := y) \propto \exp(\mathbb{E}_{x' \sim P_D P_{Q|y}} [\log P_R(x')])$$

which yields the complete AIF objective below

$$\begin{aligned} L(x, P_W, P_Q) = & \mathbb{E}_{y, s \sim P_Q} [\log P_D(x|y, s)] + \mathbb{E}_{y, s \sim P_Q} [\log P_0(s|y)] \quad (2) \\ & + \mathbb{E}_{x' \sim P_D P_Q} [\log P_R(x')] + \mathbb{H}[P_Q]. \end{aligned}$$

See Section A.5 for the intermediate derivation steps.

Next, we connect the minimalist derivation presented above to the control setting. We exploit the factorization in Eq. 1 to simplify the ELBO further. The world model of an AIF agent comprises a policy variable π to represent actions and the latent embedding (S, S') that represents the current perceptions by S and the future perceptions by S' . AIF theory assumes that these variables factorize as:

$$\begin{aligned} P_W(X', S', S, \pi | X, A) \triangleq & P_D(X'|S') P_M(S'|S, A) P_E(S|X) P_0(\pi) \end{aligned}$$

where P_M is a latent state transition kernel, P_E is an encoder that maps the sensory stimulus space to the latent perception space, P_D is a decoder that maps in the reverse direction, and P_A is a policy distribution. Let us assume an approximate posterior

$$P_Q(S, S', \pi) \triangleq P_M(S'|S, A) P_E(S|X) P_A(\pi|X)$$

that shares the same transition kernel and encoder with the world model. Such a choice of approximate posterior is standard in the probabilistic state-space modeling literature (Doerr et al., 2018) and is used to eliminate the latent overshooting term in the Dreamer model family (Hafner et al., 2020a; 2025). With this approximate posterior, the term $\mathbb{E}_{y, s \sim P_Q} [\log P_0(s|y)]$ developed in Eq. 2 drops and we get:

$$\begin{aligned} L(x, a, x', P_W, P_Q) = & \mathbb{E}_{S' \sim P_M P_E | x, a} [\log P_D(x'|S')] \\ & + \mathbb{E}_{x'', \pi \sim P_D P_M P_E P_A | x'} [\log P_R(x''|x', \pi(x'))] \quad (3) \\ & + \mathbb{H}[P_A | x']. \end{aligned}$$

In RL terms, this ELBO prescribes a Dyna-style model-based approach. The first term learns the state transition dynamics from observed triples (x, a, x') . The remaining two terms can be viewed as maximum-entropy policy search (Haarnoja et al., 2018a;b) on the estimated transition model. The formulation can be straightforwardly extended to the case where x'' is an arbitrarily long trajectory.

3. Push-forward Reinforcement Learning

We project AIF onto the distributional RL framework via a model-based extension of policy iteration presented in Algorithm 1, which augments standard policy iteration with a model update step. It performs policy updates by Bellman backups using the following operator, where the backup

Algorithm 1 Model-Based Policy Iteration (MBPI)

```

Input:  $\pi_0, i := 0$ 
while True do
    Model Update:
         $P_{i+1} := \arg \max_P \{$ 
             $\mathbb{E}_{x \sim \mathcal{U}(\mathcal{X})} \mathbb{E}_{x' \sim P_*(\cdot | x, \pi_i(x))} [\log f_P(x'|x, \pi_i(x))] \}$ 
    Policy Evaluation:
         $Q_{i+1} :=$ 
            
$$\arg \min_Q \mathbb{E}_{x \sim \mathcal{U}(\mathcal{X})} \left[ (T_{P_{i+1}}^{\pi_i} Q(x, \pi_i(x)) \right. \\ \left. - Q(x, \pi(x)))^2 \right]$$

    Policy Improvement:
         $\pi_{i+1} := \arg \max_{\pi} \mathbb{E}_{x \sim \mathcal{U}(\mathcal{X})} [Q_{i+1}(x, \pi(x))]$ 
         $i := i + 1$ 
end while

```

transition kernel P comes from the estimated model

$$(T_P^\pi Q)(x, a) \triangleq \begin{aligned} & R(x, a) + \gamma \mathbb{E}_{x' \sim P(\cdot | x, a)} [Q(x', \pi(x'))] \quad (4) \end{aligned}$$

where $Q : \mathcal{X} \times \mathcal{A} \rightarrow \mathbb{R}$ is an arbitrary function. The use of $\mathcal{U}(\mathcal{X})$ in Algorithm 1 is an idealized full-coverage assumption; in practice, x is drawn from the state distribution induced by the data (e.g., under a behavior policy). Viewed this way, MBPI is best seen as a template that highlights design choices shared by modern model-based RL. For instance, PSRL samples an MDP from the posterior and solves it (Osband et al., 2013); PILCO combines model learning with policy search (Deisenroth & Rasmussen, 2011); and Dreamer couples model learning with actor-critic updates (Hafner et al., 2020a). We temporarily suppress the policy entropy maximization in Eq. 3 for notational brevity. With finite samples and finite backups, the algorithm inherits the properties of Approximate Policy Iteration (API), which can be viewed as a two-error scheme (Bertsekas & Tsitsiklis, 1996, Prop. 6.2): each iteration incurs (i) a policy-evaluation error ε and (ii) an approximate greedification error δ , yielding asymptotic suboptimality on the order of $(\delta + 2\gamma\varepsilon)/(1-\gamma)^2$. In API, ε and δ are controlled from data; worst-case guarantees such as $|Q(x, a) - \mathbb{E}[\mathbf{G}_{x, a}^\pi]|_\infty \leq \varepsilon$ typically demand accurate estimates over a sufficiently large set of states, so the total sampling burden is dominated by the size of that set. For high-dimensional (vector) state spaces, $|\mathcal{S}|$ can grow rapidly with dimension under discretization, motivating learned state abstractions that group states with similar transition dynamics in a latent embedding (Li et al., 2006; Abel et al., 2016; 2018).

As the second step, we generalize the distributional RL framework to the case in which the transition dynamics are explicitly identified as an intermediate step and then pushed forward on the trajectory measures. Approaching RL from a probabilistic perspective, this decomposition will

pave the way to integrate AIF into the distributional RL framework. Since the return functional $\mathbf{G}_{x,a}^\pi(\omega)$ operates on a state-action trajectory ω , its distribution (therefore expectation) can be expressed through a probability measure over trajectories. We construct such a measure below.

Let $P_\pi(B|x) \triangleq P(B|x, \pi(x))$ be a Markov kernel induced by applying a policy $\pi : \mathcal{X} \rightarrow \mathcal{A}$ to a controlled Markov process with transition kernel P for $B \in \sigma(\mathcal{X})$. Define a cylinder set of length n for measurable sets $B_1, B_2, \dots, B_n \in \sigma(\mathcal{X})$ as

$$C = \{(x_1, x_2, \dots) \in \mathcal{X}^{\mathbb{N}_+} : x_1 \in B_1, x_2 \in B_2, \dots, x_n \in B_n\}.$$

According to the Ionescu-Tulcea theorem (Ionescu-Tulcea, 1949), there exists a unique probability measure $\mathbb{P}_{x_0, a_0}^{P_\pi}$ defined on the product σ -algebra $\sigma(\mathcal{X})^{\otimes \mathbb{N}_+}$ such that for every $n \in \mathbb{N}_+$ and every cylinder set C of the form $B_1 \times B_2 \times \dots \times B_n \times \mathcal{X} \times \dots$, with $B_t \in \sigma(\mathcal{X})$ for $t \geq 1$, the measure is consistent with:

$$\begin{aligned} \mathbb{P}_{x_0, a_0}^{P_\pi}(C) &= \int_{B_1} P(dx_1|x_0, a_0) \times \int_{B_2} P_\pi(dx_2|x_1) \\ &\quad \times \int_{B_3} P_\pi(dx_3|x_2) \times \dots \times \int_{B_n} P_\pi(dx_n|x_{n-1}). \end{aligned}$$

This measure defines the *canonical process* $(X_n)_{n \geq 1}$ on the path space $\mathcal{X}^{\mathbb{N}_+}$, where $X_n(\omega) \triangleq \omega_n$ for all $n \geq 1$. Here ω_n indicates the n 'th coordinate of the trajectory. The resulting triple $(\mathcal{X}^{\mathbb{N}_+}, \sigma(\mathcal{X})^{\otimes \mathbb{N}_+}, \mathbb{P}_{x_0, a_0}^{P_\pi})$ constitutes a valid probability space for the infinite-horizon controllable Markov process that starts from $P(\cdot|x_0, a_0)$ and proceeds with the policy-induced kernel P_π . We will refer to objects like $\mathbb{P}_{x_0, a_0}^{P_\pi}$ as *Markov process measures*.

Let $(E, \sigma(E))$ be a new measurable space and $f : \mathcal{X} \rightarrow E$ be a measurable map. We extend this to the infinite-horizon path space by defining the sequence-valued map $\mathbf{F} : \mathcal{X}^{\mathbb{N}_+} \rightarrow E^{\mathbb{N}_+}$ as $\mathbf{F}(\omega) = (f(x_1), f(x_2), \dots)$ where $\omega = (x_1, x_2, \dots)$ is an element of the path space $\mathcal{X}^{\mathbb{N}_+}$. We refer to objects like \mathbf{F} as *push-forward process functionals*. If we push a Markov process measure forward with this functional, we get the following measure on the observation path space $(E^{\mathbb{N}_+}, \sigma(E)^{\otimes \mathbb{N}_+})$:

$$\begin{aligned} \mathbf{F}_\# \mathbb{P}_{x_0, a_0}^{P_\pi} &\triangleq \mathbb{P}_{x_0, a_0}^{P_\pi}(\mathbf{F}^{-1}(B)) \\ &= \mathbb{P}_{x_0, a_0}^{P_\pi}\{\omega \in \mathcal{X}^{\mathbb{N}_+} : \mathbf{F}(\omega) \in B\} \end{aligned}$$

for any measurable set $B \in \sigma(E)^{\otimes \mathbb{N}_+}$. Under this definition, the measure $(\mathbf{G}_{x_0, a_0}^\pi)_\# \mathbb{P}_{x_0, a_0}^{P_\pi}$ corresponds precisely to the *return distribution* on the measurable space $(\mathbb{R}, \mathcal{B}(\mathbb{R}))$. For any Borel set $B \in \mathcal{B}(\mathbb{R})$, this measure can be expressed as:

$$\begin{aligned} \mathbb{P}_{x_0, a_0}^{P_\pi} \left(\left\{ \omega \in \mathcal{X}^{\mathbb{N}_+} : \right. \right. \\ \left. \left. R(x_0, a_0) + \sum_{t=1}^{\infty} \gamma^t R(x_t, \pi(x_t)) \in B \right\} \right). \end{aligned}$$

The return distributions induced by two different Markov kernels P and P' can then be expressed as $(\mathbf{G}_{x_0, a_0}^\pi)_\# \mathbb{P}_{x_0, a_0}^{P_\pi}$ and $(\mathbf{G}_{x_0, a_0}^\pi)_\# \mathbb{P}_{x_0, a_0}^{P'}$, respectively.

We can define the distributional counterpart of the generalized Bellman operator introduced in Eq. 4 with a specific Markov kernel P as follows:

$$\mathbf{T}_P^\pi \eta_{x,a} \triangleq R(x, a) + \gamma \mathbb{E}_{x' \sim P(x'|x, a)} [\eta_{x', \pi(x')}]$$

for a real-valued probability measure $\eta_{x,a} : \mathcal{X} \times \mathcal{A} \rightarrow \mathcal{P}_{\mathbb{R}}$ conditioned on $(x, a) \in \mathcal{X} \times \mathcal{A}$. Define the maximal form of the p -Wasserstein distance $\bar{\mathcal{W}}_p(P, \bar{P}) \triangleq \sup_{x,a} \mathcal{W}_p(P_{x,a}, \bar{P}_{x,a})$ where $P_{x,a}$ and $\bar{P}_{x,a}$ are two probability measures on the same space as $\eta_{x,a}$. We can re-express the contraction property of the distributional Bellman operator (Bellemare et al., 2017) in terms of push-forwards of Markov process measures.

Lemma 3.1. *Let $P_\pi, \bar{P}_\pi, P_\pi^*$ be Markov kernels induced by a fixed policy π and \mathbf{F} be a push-forward process functional, then the distributional Bellman operator $\mathbf{T}_{P_\pi^*}^\pi$ is a contraction with respect to $\bar{\mathcal{W}}_p$*

$$\bar{\mathcal{W}}_p \left(\mathbf{T}_{P_\pi^*}^\pi \mathbf{F}_\# \mathbb{P}^{P_\pi}, \mathbf{T}_{P_\pi^*}^\pi \mathbf{F}_\# \mathbb{P}^{\bar{P}_\pi} \right) \leq \gamma \bar{\mathcal{W}}_p \left(\mathbf{F}_\# \mathbb{P}^{P_\pi}, \mathbf{F}_\# \mathbb{P}^{\bar{P}_\pi} \right).$$

The key nuance here is that the contraction modulus is due to γ within the distributional Bellman operator, not to the discount factor applied by the return functional. From Banach's fixed point theorem (Banach, 1922), it follows straightforwardly that there exists $\hat{P}_\pi \in \mathcal{P}_{\mathcal{X}}$ that satisfies $\bar{\mathcal{W}}_p(\mathbf{T}_{P_\pi^*}^\pi \mathbf{F}_\# \mathbb{P}^{\hat{P}_\pi}, \mathbf{F}_\# \mathbb{P}^{\hat{P}_\pi}) = 0$ for a sufficiently large set of admissible Markov kernels $\mathcal{P}_{\mathcal{X}}$. One can find this fixed point at a geometric rate (i.e., the error is $O(\gamma^k)$) by starting from an arbitrary $P_\pi^0 \in \mathcal{P}_{\mathcal{X}}$ and repeatedly applying $\mathbf{T}_{P_\pi^*}^\pi$. It is important to remark that this fixed point is unique in the space of Markov process measures after a push-forward with functional \mathbf{F} . There may be multiple Markov process measures almost surely equal to the fixed point $\mathbf{F}_\# \mathbb{P}_{x_0, a_0}^{P_\pi}$ after being pushed forward with \mathbf{F} . Obviously, $\mathbf{F}_\# \mathbb{P}_{x_0, a_0}^{P_\pi^*}$ also satisfies this condition. The Markov kernel of the Bellman operator plays the role of an anchor in the search process performed via Bellman backups.

The advantage of distributional RL over model-based RL appears in situations where capturing the push-forward of the Markov process measure with the return functional is sufficient for decision making, such as in risk-sensitive RL (Lim & Malik, 2022; Keramati et al., 2020; Dabney et al., 2018a; Bernhard et al., 2019). The equivalence of this measure within a set of transition kernels brings sample efficiency when it can be exploited by the learning algorithm. Model-based RL theory formulates such equivalence classes via *state abstractions* (Li et al., 2006; Givan et al., 2003; Jiang et al., 2015). We will next develop some essential concepts

to establish the link between state abstractions and distributional RL. First, we need to construct an embedding space on which state abstractions can be formulated.

Definition 3.2. A mapping $K : \mathcal{S} \rightarrow \mathcal{P}_{\mathcal{X}}$ is said to be an **L -Lipschitz Markov kernel** if (i) for every $B \in \sigma(\mathcal{X})$, $s \mapsto K(s, B)$ is measurable and (ii) for all $s_1, s_2 \in \mathcal{S}$: $\mathcal{W}_p(K(s_1, \cdot), K(s_2, \cdot)) \leq L \cdot |s_1 - s_2|$. The action of the kernel K on a measure $P \in \mathcal{P}_{\mathcal{S}}$, denoted KP , is the measure on \mathcal{X} defined by:

$$(KP)(B) \triangleq \int_{\mathcal{S}} K(s, B) P(ds), \quad \forall B \in \sigma(\mathcal{X}).$$

Now consider the push-forward of the transition kernel P of a Markov process $\mathbb{P}_{x,a}^P$ with an L_E -Lipschitz continuous function S to an embedding space \mathcal{S} , which we denote by $S_{\#}P$, and then mapping back to the state space by an L_D -Lipschitz Markov kernel P_D . This composite operation can be viewed as the action of P_D on the measure $S_{\#}P$. We can also construct the same outcome by transforming the input of P_D , which then defines an operator on P .

Definition 3.3. Let $F : \mathcal{X} \rightarrow \mathcal{S}$ be a measurable transformation, and let $K : \mathcal{S} \rightarrow \mathcal{P}_{\mathcal{X}}$ be an L -Lipschitz Markov kernel. We define the **composite kernel operator** $(KF) : \mathcal{X} \rightarrow \mathcal{P}_{\mathcal{X}}$ pointwise as $K(x, \cdot) = K(F(x), \cdot)$. For any measure $P \in \mathcal{P}_{\mathcal{X}}$, the action of the operator KF is given by:

$$(KF P)(B) \triangleq \int_{\mathcal{X}} K(F(x), B) P(dx), \quad \forall B \in \sigma(\mathcal{X}).$$

The key observation is that the action of $(KF P)$ is identical to that of $K(F_{\#}P)$. The following result establishes how the Lipschitz continuity of a Markov kernel is affected by an input transformation.

Lemma 3.4. Let $F : \mathcal{X} \rightarrow \mathcal{S}$ be an M -Lipschitz transformation and $K : \mathcal{S} \rightarrow \mathcal{P}_{\mathcal{X}}$ be an L -Lipschitz Markov kernel. Then the composite kernel operator $(KF) : \mathcal{X} \rightarrow \mathcal{P}_{\mathcal{X}}$ is an $(L \cdot M)$ -Lipschitz Markov kernel.

Our main theoretical result follows straightforwardly from the fact that transforming the transition kernels of two Markov processes with a point-wise fixed L -Lipschitz operator contracts their probability measures by a factor of L with respect to the p -Wasserstein distance. The consequence in our context is that performing distributional RL after an auto-encoding operation with an L_E -Lipschitz encoder $S_{\#}P$ and an L_D -Lipschitz decoder P_D affects the contraction modulus by $L_E \cdot L_D$.

Theorem 3.5. Let $P_{\pi}, \bar{P}_{\pi}, P_{\pi}^* \in \mathcal{P}_{\mathcal{X}}$ and \mathbf{F} be a push-forward process functional. Let P_D be an L_D -Lipschitz Markov kernel and $S : \mathcal{X} \rightarrow \mathcal{S}$ be a L_E -Lipschitz continuous measurable map from $(\mathcal{X}, \sigma(\mathcal{X}))$ to $(\mathcal{S}, \sigma(\mathcal{S}))$. Then

the following inequality holds for any $x_0, a_0 \in \mathcal{A}, \mathcal{X}$

$$\begin{aligned} \bar{\mathcal{W}}_p \left(\mathbf{T}_{P_{\pi}}^{\pi} \mathbf{F}_{\#} \mathbb{P}_{x_0, a_0}^{(P_D S) P_{\pi}}, \mathbf{T}_{P_{\pi}^*}^{\pi} \mathbf{F}_{\#} \mathbb{P}_{x_0, a_0}^{(P_D S) \bar{P}_{\pi}} \right) \\ \leq \gamma \cdot L_E \cdot L_D \cdot \bar{\mathcal{W}}_p \left(\mathbf{F}_{\#} \mathbb{P}_{x_0, a_0}^{P_{\pi}}, \mathbf{F}_{\#} \mathbb{P}_{x_0, a_0}^{\bar{P}_{\pi}} \right). \end{aligned}$$

When a narrow information bottleneck yields an efficient compression in the embedding space, L_D should be small as the returns will create large equivalence classes in the latent trajectory space (see Figure 3 in the appendix), which will reduce the contraction modulus of the Bellman backups and speed up convergence. We can let distributional RL inherit these benefits of AIF by expressing an auto-encoding operation within that framework. Let us redefine $\mathbf{G}_{\#} \mathbb{P}_{x_0, a_0}^{(P_D S) P_{\pi}}$ in terms of an *encoding process* defined on the latent space and a *decoding process* that maps back to the observation space. The encoding process on $\mathcal{S}^{\mathbb{N}_+}$ pushes $P_{x_0, a_0}^{P_{\pi}}$ forward through the sequence map $\mathbf{S}(\omega) = (S(x_1), S(x_2), \dots)$, which leads to a new measure $\mathbf{S}_{\#} \mathbb{P}_{x_0, a_0}^{P_{\pi}}$ on the space $(\mathcal{S}^{\mathbb{N}_+}, \sigma(\mathcal{S})^{\otimes \mathbb{N}_+})$. For any sequence $\mathbf{s} = (s_1, s_2, \dots) \in \mathcal{S}^{\mathbb{N}_+}$, the kernel P_D induces a conditional path measure $\mathbb{P}_{P_D | \mathbf{s}}$ on $\mathcal{X}^{\mathbb{N}_+}$ via Ionescu-Tulcea:

$$\mathbb{P}^{P_D | \mathbf{s}}(C) \triangleq \int_{B_1} P_D(dx_1 | s_1) \times \dots \times \int_{B_n} P_D(dx_n | s_n).$$

This represents the stochastic *decoding* of the representation path back into the state space. The return distribution can now be expressed as an integration over the intermediate measure $\mathbf{S}_{\#} \mathbb{P}_{x_0, a_0}^{P_{\pi}}$ in the space $\mathcal{S}^{\mathbb{N}_+}$. Defining the expected return of a fixed representation path \mathbf{s} as

$$(\mathbf{G}_{x_0, a_0}^{\pi})_{\#} \mathbb{P}^{P_D | \mathbf{s}}(B) \triangleq \mathbb{P}^{P_D | \mathbf{s}} \left(\left\{ \omega \in \mathcal{X}^{\mathbb{N}_+} : R(x_0, a_0) + \sum_{t=1}^{\infty} \gamma^t R(x_t, \pi(x_t)) \in B \right\} \right)$$

we can express the final return distribution as the integral of these local returns over the representation measure:

$$(\mathbf{G}_{x_0, a_0}^{\pi})_{\#} \mathbb{P}_{x_0, a_0}^{(P_D S) P_{\pi}}(B) = \int_{\mathcal{S}^{\mathbb{N}_+}} (\mathbf{G}_{x_0, a_0}^{\pi})_{\#} \mathbb{P}^{P_D | \mathbf{s}}(B) \mathbf{S}_{\#} \mathbb{P}_{x_0, a_0}^{P_{\pi}}(d\mathbf{s}). \quad (5)$$

The fact that the outcome is a composite measure will be instrumental in its implementation.

Let us next demonstrate how this result translates to a distributional RL algorithm. Although our result has more general implications, we will follow the established framework that performs Bellman residual minimization with respect to \mathcal{W}_2 for policy evaluation and a policy update on the expectation of the fitted return distribution. Formally,

Algorithm 2 Push-Forward Policy Iteration (PPI)

```

Input:  $\pi_0, i := 0$ 
while True do
    for  $x \in \mathcal{X}$  do
         $Z_{x,a}^{i+1} := \arg \min_{Z \in \mathcal{Z}_{x,a}^{\pi_i}} \mathbb{E}_{\tau \sim \mathcal{U}(0,1)} \mathbb{E}_{s \sim Z_{x,a}} \left[ \left( F_{(\mathbf{G}_{x,a}^{\pi_i}) \# \mathbb{P}_{x,a}^{\pi_i}}^{-1}(\tau) - F_{\mathbf{T}_{P_*}^{\pi_i}(\mathbf{G}_{x',\pi_i(x')}^{\pi_i}) \# \mathbb{P}_{x',\pi_i(x')}^{\pi_i}}^{-1}(\tau) \right)^2 \right]$ 
         $\pi_{i+1}(x) := \arg \max_{a \in \mathcal{A}} \mathbb{E}_{s \sim Z_{x,a}^{i+1}} \left[ (\mathbf{G}_{x,a}^{\pi_i}) \# \mathbb{P}_{x,a}^{\pi_i}(s) \right]$ 
         $i := i + 1$ 
    end for
end while

```

the policy evaluation step minimizes the objective below

$$J(P_\pi) \triangleq \mathbb{E}_{x \sim \mathcal{U}(\mathcal{X})} [\mathcal{W}_2^2((\mathbf{G}_{x_0,a_0}^{\pi_i}) \# \mathbb{P}_{x_0,a_0}^{P_\pi}, \mathbf{T}_{P_*}^{\pi_i}(\mathbf{G}_{x',\pi(x')}^{\pi_i}) \# \mathbb{P}_{x',\pi(x')}^{P_\pi})].$$

Since $\mathbf{T}_{P_*}^{\pi_i}$ has a unique fixed point, we have $J(\widehat{P}_\pi) = 0$. When the Markov process is transformed by an auto-encoder $P_D S$ we attain the following upper bound to this objective

$$\begin{aligned} J(S) &\triangleq \mathbb{E}_{x \sim \mathcal{U}(\mathcal{X})} [\mathcal{W}_2^2((\mathbf{G}_{x_0,a_0}^{\pi_i}) \# \mathbb{P}_{x_0,a_0}^{(P_D S) P_\pi}, \mathbf{T}_{P_*}^{\pi_i}(\mathbf{G}_{x',\pi(x')}^{\pi_i}) \# \mathbb{P}_{x',\pi(x')}^{(P_D S) P_\pi})] \\ &\leq \mathbb{E}_{x \sim \mathcal{U}(\mathcal{X})} \left[\mathbb{E}_{s \sim \mathbf{S} \# \mathbb{P}_{x_0,a_0}^{P_\pi}} \left[\mathbb{E}_{\tau \in \mathcal{U}(0,1)} \left[\left(F_{(\mathbf{G}_{x_0,a_0}^{\pi_i}) \# \mathbb{P}_{x_0,a_0}^{\pi_i}}^{-1}(\tau) - F_{\mathbf{T}_{P_*}^{\pi_i}(\mathbf{G}_{x',\pi(x')}^{\pi_i}) \# \mathbb{P}_{x',\pi(x')}^{\pi_i}}^{-1}(\tau) \right)^2 \right] \right] \right]. \end{aligned}$$

As the final statement is indexed only by $\mathbf{S} \# \mathbb{P}_{x_0,a_0}^{P_\pi}$, we can instead search directly the space of encoding measures

$$\mathcal{Z}_{x,a}^\pi \triangleq \{Z_{x,a} : Z_{x,a} = \mathbf{S} \# \mathbb{P}_{x_0,a_0}^{P_\pi}, P_\pi \in \mathcal{P}_\pi\} \quad (6)$$

for a state-action pair $(x, a) \in \mathcal{X} \times \mathcal{A}$. Using the expectation of the identified push-forward distributions in the policy improvement step, which is the Bayes-optimal way to make predictions with it, we arrive at Algorithm 2. We call this algorithm template *push-forward policy iteration* and its practical applications *push-forward reinforcement learning*. This algorithm will deliver a policy sequence identical to Algorithm 1 whenever $(\mathbf{G}_{x_0,a_0}^{\pi_i}) \# \mathbb{P}_{x_0,a_0}^{P_\pi}$ is realizable under $\mathcal{Z}_{x,a}^\pi$ for all x, a, π , as this will make their policy improvement steps measurably identical. In practice, this realizability can be enforced with powerful function approximators. The gain in sample complexity depends on the trade-off between the capacity of these function approximators and the level of compression that the underlying transition dynamics permits via state abstractions.

4. Active Inference with Push-Forward RL

We next integrate AIF into the push-forward RL framework and remove the need to estimate the transition kernel of the

underlying dynamical system. We will exploit the fact that in Eq. 3, P_M and P_E always appear together in a marginalization process. Let us denote their marginal by

$$P_{S|x,a}(S') \triangleq \mathbb{E}_{s \sim P_{E|x}} [P_M(S'|s, a)].$$

This distribution can be interpreted as a *transfer transition kernel* from a source Markov chain defined on \mathcal{X} to a target Markov chain defined on \mathcal{S} (Lazaric & Restelli, 2011). Note that P_S can be viewed as a push-forward of an underlying P_π with some function S .

Let us next define the next state S' as the infinitely-long trajectory of future latent states s simulated on the world model after taking action a at state x and following policy π afterwards. Let ω be the corresponding states in the observation space. We can then construct the desired state distribution as the return of this trajectory: $P_R(\omega) \propto \exp((\mathbf{G}_{x,a}^{\pi_i}) \# (\omega))$. Placing this construction into the related term of the ELBO developed in Equation (3) we get

$$\begin{aligned} &\mathbb{E}_{\omega \sim P_D P_M P_E | x, a} [(\mathbf{G}_{x,a}^{\pi_i}) \# (\omega)] \\ &= \mathbb{E}_{\omega \sim \mathbb{P}_{x,a}^{(P_D P_M P_E) \pi}} [(\mathbf{G}_{x,a}^{\pi_i}) \# (\omega)] \\ &= \mathbb{E}[(\mathbf{G}_{x,a}^{\pi_i}) \# \mathbb{P}_{x,a}^{(P_D P_M P_E) \pi}] \\ &= \mathbb{E}_{s \sim \mathbf{S} \# \mathbb{P}_{x,a}^{P_\pi}} \left[(\mathbf{G}_{x,a}^{\pi_i}) \# \mathbb{P}_{x,a}^{P_\pi} \right] \\ &= \mathbb{E}_{\omega \sim P_D P_S | x, a} [(\mathbf{G}_{x',\pi(x')}^{\pi_i}) \# (\omega)] \end{aligned}$$

where we omit the integral over P_A for notational brevity. The first and the fourth equations follow from definitions, the second from the Law of the Unconscious Statistician (LOTUS), and the third from Eq. 5. By learning an encoding process as in Equation (6) and performing distributional RL on the latent trajectory space, we can capture $(\mathbf{G}_{x,a}^{\pi_i}) \# \mathbb{P}_{x,a}^{P_\pi}$. Thus, we can inherit the benefits of learning a transition kernel as in Algorithm 1 to simulate trajectories. Furthermore, we can quantify the effects of downstream calculations on these simulations in an infinitely long horizon.

We can implement this recipe by learning a state-action amortized encoder that maps to the latent space and performing quantile regression of returns on this space. To operate on a latent space, we need to cast the quantile regression problem as a maximum likelihood estimation instance and assign input-dependent priors to its parameters. The solution of the problem below for an i.i.d. sample of Y gives an unbiased estimate of the τ 'th quantile of a conditional distribution $P(Y|X)$ with input X and output Y :

$$\widehat{g}_\tau \triangleq \arg \min_{g_\tau} \mathbb{E}_{X,Y \sim P} [\ell_\tau(Y - g_\tau(X))] \quad (7)$$

for a predictor g_τ where $\ell_\tau(u) \triangleq (|u| + (2\tau - 1)u)/2$ is the check loss. By extending the connection established by Yu & Moyeed (2001), we can frame \widehat{g}_τ as the maximum likelihood estimate (MLE) of the Asymmetric Laplace

Algorithm 3 Distributional Active Inference (DAIF)

```

Input:  $P_A$ 
 $x = \text{env.reset}()$ 
while True do
     $\pi \sim P_A(\cdot|x)$ ,  $a := \pi(x)$ 
     $x' := \text{env.step}(a)$ 
     $D := D \cup (x, a, x')$ 
    repeat
         $(x, a, x') \sim D$ ,  $\tau \sim \mathcal{U}(0, 1)$ ,  $\pi \sim P_A(\cdot|x)$ 
         $\phi := \arg \max_{\phi'} \left\{ \mathbb{E}_{\mu_\tau, \sigma_\tau^2 \sim E_{\phi'}(x, a, \tau)} [\log f_\tau(\right.$ 
             $R(x, a) + \gamma \mathbb{E}_{\mu'_\tau \sim E_{\phi'}(x', \pi(x'), \tau)} [\mu'_\tau] | \mu_\tau, \sigma_\tau^2)] \left. \right\}$ 
         $P_A := \arg \max_{P'_A} \left\{ \mathbb{E}_{\pi \sim P'_A(\cdot|x)} [\right.$ 
             $\mathbb{E}_{\mu_\tau \sim E_{\phi'}(x, \pi(x), \tau)} [\mu_\tau]] \left. \right] + \mathbb{H}[P'_A] \right\}$ 
    until end of training epoch
end while

```

Distribution (ALD) (Koenker & Bassett Jr, 1978)

$$f_\tau(Y|X; g_\tau, \sigma_\tau) = \frac{\tau(1-\tau)}{\sigma_\tau} \exp\left(-\frac{\ell_\tau(Y - g_\tau(X))}{\sigma_\tau}\right).$$

By setting $\mu_\tau \triangleq g_\tau$ and treating both μ_τ and σ_τ as random variables that follow a prior distribution with state and action dependent hyperparameters, we can perform distributional reinforcement learning on a latent space. We can capture the randomness caused by the auto-encoding step with a probability measure $E_\phi(x, a, \tau)$, the parameters ϕ of which are trainable with a high-capacity function approximator. In our context, μ_τ captures the mean quantile for these returns and σ_τ their standard deviation. The regression target Y can be evaluated via Bellman backups.

The remaining two terms of the AIF ELBO perform a model update and policy entropy maximization. Whether to implement the latter is a design choice. We obtained better results with action-noise exploration than maximum entropy policy search (see Appendix B.1.4, Table 6). This is expected, as the other steps of our uncertainty quantification pipeline already induce the necessary randomness for exploration. As the model update is a lower bound to the same step of Algorithm 1, the same consequences of Lemma 3.1 apply.

With this we end up with Algorithm 3, which we refer to as *Distributional Active Inference (DAIF)*. This algorithm preserves the benefits of performing AIF whenever they are available in its native model-based version while eliminating the need to learn a transition kernel. A natural choice for E_ϕ would be the Normal-Inverse Gamma distribution with parameterized inputs. However, this would not permit an analytical calculation of the expectation of $\log p_\tau$ in the policy evaluation step. Having observed in our preliminary implementations that modeling the uncertainty around μ_τ

does not improve performance, we instead assumed a normal prior on the mean with fixed variance and modeled an Inverse Gamma prior for σ_τ (see Section B.2.4).

5. The Prior Art of RL with Active Inference

AIF casts control as inference, selecting policies that minimize expected free energy (EFE), with epistemic terms inducing principled exploration (Friston et al., 2009; 2015). Most practical AIF agents are *model-based*: they learn an explicit world model and use variational inference to maintain beliefs and/or evaluate EFE, often with planning or lookahead (Ueltzhöffer, 2018; Çatal et al., 2019; Tschantz et al., 2020a; Fountas et al., 2020; Paul et al., 2021; Mazzaglia et al., 2021; Schneider et al., 2022). Complementary work analyzes links and limitations between AIF and RL/control-as-inference, including when EFE objectives recover RL-like optimality or reduce to standard intrinsic-motivation criteria (Millidge et al., 2020; Millidge, 2020; Sajid et al., 2021a; Da Costa et al., 2023). Closest to our work, Malekzadeh & Plataniotis (2024) derive Bellman-style EFE recursions for POMDPs and develop actor-critic updates in belief space, but still rely on learned belief representations and a world model. DAIF sidesteps world-model learning for EFE evaluation by learning targets directly from sampled transitions. See Section C for an extended review.

6. Experiments

AIF postulates that the action-perception cycle of a biological agent is mediated by simulations on a latent space (Parr et al., 2022). Since the latent space applies state abstractions to maximize simulation efficiency, the advantages of AIF should be observed in scenarios where state abstractions facilitate the learning task. We represent such a use case with a two-dimensional grid world environment whose transition probabilities share the dynamics of the RiverSwim (Osband et al., 2013) setup on a one-dimensional latent manifold unknown to the agent. See Section B.1 and Figure 3 for further details. Figure 2 (right panel) demonstrates that both model-based RL and vanilla distributional RL fail to solve the task as the problem horizon grows, whereas our DAIF maintains its performance. As shown in the left panel, the models behave similarly in long problem horizons when state abstractions are not advantageous.¹

We also adapt DAIF to continuous control with deep actor-critics (Section B.2.4). As summarized in Table 1, DAIF provides consistent performance gains across various environments from three benchmark suites. Controlling

¹We choose the policy iteration variant of the Posterior Sampling for Reinforcement Learning (PSRL) due to its competitive empirical performance (Tiapkin et al., 2022, Figure 1), although its regret profile is not yet fully characterized.

Table 1. Ranking comparison on 19 continuous control environments from three benchmark suites. The algorithms are ranked separately for each repetition of each environment. The sign \pm indicates the standard deviation. Area Under the Learning Curve (AULC) measures sample efficiency and Final Return measures how well a control task has been solved. The method with the smallest rank value is marked in bold. As the architecture and hyperparameters of the original DrQ-v2 (Yarats et al., 2022) is tuned specifically for visual control, we do not evaluate this model in the other two benchmark suites. **# Envs:** Number of environments. **# Reps:** Number of experiment replications.

Suite	# Envs	# Reps	Area Under the Learning Curve (AULC)					Final Return				
			DRND	DRQv2	DSAC	DTD3	DAIF	DRND	DRQv2	DSAC	DTD3	
EvoGym	7	10	3.2 \pm 1.1	—	2.9 \pm 0.8	2.0 \pm 0.8	1.5 \pm 0.7	3.7 \pm 0.7	—	2.8 \pm 0.8	2.0 \pm 0.8	1.6 \pm 0.8
DMC	7	10	3.2 \pm 1.1	—	2.8 \pm 0.9	2.4 \pm 1.0	1.6 \pm 0.7	3.1 \pm 1.2	—	2.8 \pm 0.8	2.6 \pm 0.9	1.5 \pm 0.8
DMC Vision	5	5	4.2 \pm 1.3	3.5 \pm 1.1	2.5 \pm 1.1	2.9 \pm 1.2	1.9 \pm 1.2	4.4 \pm 1.0	3.0 \pm 1.2	2.8 \pm 1.1	3.8 \pm 1.2	2.0 \pm 1.4

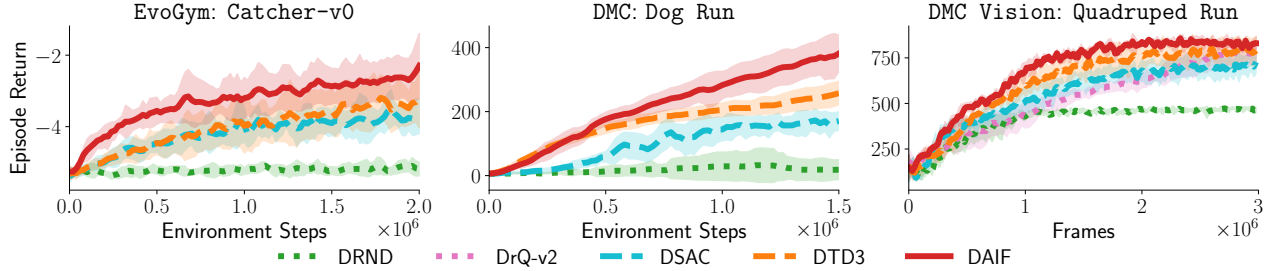


Figure 1. Evaluation curves for three representative environments, one per suite, where DAIF clearly improves the state of the art. These are relatively harder problems of the related suite due to either complex dynamics or large state or action dimensionality, where the abstraction of the return distribution is beneficial. DAIF performs comparably to the state of the art when it does not improve. For the learning curves of the remaining environments, see Section B.2.

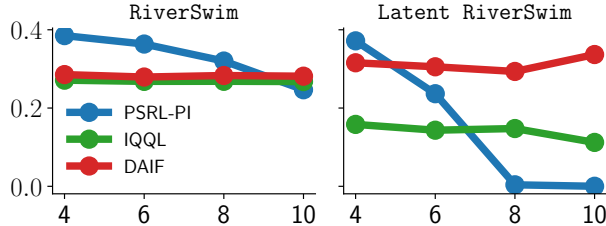


Figure 2. Horizontal axis: Distance from the initial state to the most desired state. **Vertical axis:** Frequency of the visitation of the most desired state. DAIF matches the plain distributional RL performance when transition dynamics cannot be represented more efficiently in a latent space (left panel). DAIF outperforms both distributional and model-based counterparts when a latent manifold drives the dynamics at a degree increasing with the difficulty of the problem (right panel). For the learning curves of individual configurations, see Figure 4 in the appendix.

DMC locomotors is difficult due to compounding function-approximation errors that cause the deadly triad (Ciosek et al., 2019). DMC vision presents the additional challenge of controlling these platforms from the high-dimensional state space comprising raw pixels. EvoGym introduces control problems for soft robots with deformable bodies.

Figure 1 reports learning curves for one representative environment per suite. *Catcher-v0* is classified as a *hard* task in EvoGym (Bhatia et al., 2021) and has the steepest learning curve within the interaction budget. *Dog Run* has the highest state dimensionality among all DMC robots, and running demands sustained high-speed control. *Quadruped Run* has

the highest action dimensionality among the vision-based environments. DAIF outperforms state-of-the-art baselines by a clear margin throughout the entire learning process. DAIF’s pronounced performance boost corroborates our view that AIF is especially useful for controlling challenging environments with limited computational resources. The performance boost of DAIF requires about 12% more wall-clock computation time than distributional actor-critic methods. See Section B.2 for full details of these experiments.

7. Takeaways and Open Questions

We provided a new theoretical framework that enables casting AIF as a simple extension of distributional RL. This implies that the improvements in the adaptation capabilities of an AIF agent should be observed in the distributional setting. We reported a comprehensive set of experiment results that support this claim. The deep RL implementation of DAIF improved the state of the art in multiple soft robotics benchmarks and challenging visual control tasks. DAIF inherits the convergence guarantees of distributional RL with an improved contraction modulus. A rigorous characterization of its finite-sample characteristics is an open question, as it is for the distributional RL field. Our theoretical framework can also lay a foundation for a formal analysis of AIF’s computational properties. A methodology for this could be extending the sample complexity analysis of linear quadratic control (Krauth et al., 2019) to well-behaved non-linearities.

Impact Statement

This work makes both theoretical and algorithmic contributions to the general field of machine learning. The theoretical contributions are two-fold. The first is a formulation of the key concepts of distributional reinforcement learning using only stochastic process constructions and their transformations. The second is a derivation of the active inference machinery using variational and causal inference concepts in a rigorous and consistent manner. This derivation highlights a significant simplification in the resulting objective function. The algorithmic contribution is a distributional counterpart of active inference, which has thus far been practiced in computationally demanding model-based settings. We do not foresee negative societal impacts beyond those generally associated with increased automation.

References

Abel, D., Hershkowitz, D., and Littman, M. Near optimal behavior via approximate state abstraction. In *International Conference on Machine Learning*, 2016.

Abel, D., Arumugam, D., Lehnert, L., and Littman, M. State abstractions for lifelong reinforcement learning. In *International Conference on Machine Learning*, 2018.

Akgül, A., Baykal, G., Haußmann, M., and Kandemir, M. Overcoming non-stationary dynamics with evidential proximal policy optimization. *Transactions on Machine Learning Research*, 2025.

Bai, W., Zhang, C., Fu, Y., Zhao, P., and Qian, H. PACER: A fully push-forward-based distributional reinforcement learning algorithm. *Neurocomputing*, 2025.

Banach, S. Sur les opérations dans les ensembles abstraits et leur application aux équations intégrales. *Fundamenta Mathematicae*, 1922.

Barth-Maron, G., Hoffman, M. W., Budden, D., Dabney, W., Horgan, D., TB, D., Muldal, A., Heess, N., and Lillicrap, T. Distributed distributional deterministic policy gradients. In *International Conference on Learning Representations*, 2018.

Bellemare, M. G., Srinivasan, S., Ostrovski, G., Schaul, T., Saxton, D., and Munos, R. Unifying count-based exploration and intrinsic motivation. In *Advances in Neural Information Processing Systems*, 2016.

Bellemare, M. G., Dabney, W., and Munos, R. A distributional perspective on reinforcement learning. In *International Conference on Machine Learning*, 2017.

Bellemare, M. G., Dabney, W., and Rowland, M. *Distributional reinforcement learning*. MIT Press, 2023.

Bernhard, J., Pollok, S., and Knoll, A. Addressing inherent uncertainty: Risk-sensitive behavior generation for automated driving using distributional reinforcement learning. In *2019 IEEE Intelligent Vehicles Symposium (IV)*, 2019.

Bertsekas, D. P. and Tsitsiklis, J. N. *Neuro-Dynamic Programming*. Athena Scientific, 1996.

Bhatia, J., Jackson, H., Tian, Y., Xu, J., and Matusik, W. Evolution gym: A large-scale benchmark for evolving soft robots. In *Advances in Neural Information Processing Systems*, 2021.

Black, K., Brown, N., Driess, D., Esmail, A., Equi, M., Finn, C., Fusai, N., Groom, L., Hausman, K., Ichter, B., Jakubczak, S., Jones, T., Ke, L., Levine, S., Li-Bell, A., Mothukuri, M., Nair, S., Pertsch, K., Shi, L. X., Tanner, J., Vuong, Q., Walling, A., Wang, H., and Zhilinsky, U. π_0 : A vision-language-action flow model for general robot control. *arXiv preprint arXiv:2410.24164*, 2024.

Botteghi, N., Poel, M., and Brune, C. Unsupervised representation learning in deep reinforcement learning: A review. *IEEE Control Systems*, 2025.

Burda, Y., Edwards, H., Storkey, A., and Klimov, O. Exploration by random network distillation. In *International Conference on Learning Representations*, 2019.

Çatal, O., Nauta, J., Verbelen, T., Simoens, P., and Dhoedt, B. Bayesian policy selection using active inference. *arXiv preprint arXiv:1904.08149*, 2019.

Cho, T., Han, S., Lee, H., Lee, K., and Lee, J. Pitfall of optimism: distributional reinforcement learning by randomizing risk criterion. In *Advances in Neural Information Processing Systems*, 2023.

Ciosek, K., Vuong, Q. H., Loftin, R. T., and Hofmann, K. Better exploration with optimistic actor-critic. In *Advances in Neural Information Processing Systems*, 2019.

Clark, A. *The experience machine: How our minds predict and shape reality*. Random House, 2024.

Cullen, M., Davey, B., Friston, K. J., and Moran, R. J. Active inference in OpenAI Gym: A paradigm for computational investigations into psychiatric illness. *Biological psychiatry: cognitive neuroscience and neuroimaging*, 2018.

Da Costa, L., Parr, T., Sajid, N., Veselic, S., Neacsu, V., and Friston, K. Active inference on discrete state-spaces: A synthesis. *Journal of Mathematical Psychology*, 99: 102447, 2020.

Da Costa, L., Sajid, N., Parr, T., Friston, K., and Smith, R. Reward maximization through discrete active inference. *Neural Computation*, 2023.

Dabney, W., Ostrovski, G., Silver, D., and Munos, R. Implicit quantile networks for distributional reinforcement learning. In *International Conference on Machine Learning*, 2018a.

Dabney, W., Rowland, M., Bellemare, M., and Munos, R. Distributional reinforcement learning with quantile regression. In *Proceedings of the AAAI Conference on Artificial Intelligence*, 2018b.

Deisenroth, M. and Rasmussen, C. E. PILCO: A model-based and data-efficient approach to policy search. In *International Conference on Machine Learning*, 2011.

Doerr, A., Daniel, C., Schiegg, M., Duy, N.-T., Schaal, S., Toussaint, M., and Trimpe, S. Probabilistic recurrent state-space models. In *International Conference on Machine Learning*, 2018.

Döring, L., Wille, B., Birr, M., Bîrsan, M., and Slowik, M. ADDQ: Adaptive distributional double Q-learning. In *International Conference on Machine Learning*, 2025.

Dorrell, W., Latham, P. E., Behrens, T. E. J., and Whittington, J. C. R. Actionable neural representations: Grid cells from minimal constraints. In *International Conference on Learning Representations*, 2023.

Eberhardt, F. and Scheines, R. Interventions and causal inference. *Philosophy of science*, 2007.

Fountas, Z., Sajid, N., Mediano, P., and Friston, K. Deep active inference agents using monte-carlo methods. In *Advances in Neural Information Processing Systems*, 2020.

Friston, K. The free-energy principle: a rough guide to the brain? *Trends in cognitive sciences*, 2009.

Friston, K., Rigoli, F., Ognibene, D., Mathys, C., Fitzgerald, T., and Pezzulo, G. Active inference and epistemic value. *Cognitive Neuroscience*, 2015.

Friston, K., Fitzgerald, T., Rigoli, F., Schwartenbeck, P., and Pezzulo, G. Active inference: a process theory. *Neural Computation*, 2017.

Friston, K. J., Daunizeau, J., and Kiebel, S. J. Reinforcement learning or active inference? *PLOS One*, 2009.

Fujimoto, S., Hoof, H., and Meger, D. Addressing function approximation error in actor-critic methods. In *International Conference on Machine Learning*, 2018.

Givan, R., Dean, T., and Greig, M. Equivalence notions and model minimization in Markov decision processes. *Artificial Intelligence*, 2003.

Haarnoja, T., Zhou, A., Abbeel, P., and Levine, S. Soft actor-critic: Off-policy maximum entropy deep reinforcement learning with a stochastic actor. In *International Conference on Machine Learning*, 2018a.

Haarnoja, T., Zhou, A., Hartikainen, K., Tucker, G., Ha, S., Zhou, J., Kumar, V., Zhu, H., Gupta, A., Abbeel, P., and Levine, S. Soft actor-critic algorithms and applications. *arXiv preprint arXiv:1812.05905*, 2018b.

Hafner, D., Lillicrap, T., Fischer, I., Villegas, R., Ha, D., Lee, H., and Glover, J. Dream to control: Learning behaviors by latent imagination. In *International Conference on Learning Representations*, 2020a.

Hafner, D., Ortega, P. A., Ba, J., Parr, T., Friston, K., and Heess, N. Action and perception as divergence minimization. *arXiv preprint arXiv:2009.01791*, 2020b.

Hafner, D., Pasukonis, J., Ba, J., and Lillicrap, T. Mastering diverse control tasks through world models. *Nature*, 2025.

Hodson, R., Mehta, M., and Smith, R. The empirical status of predictive coding and active inference. *Neuroscience & Biobehavioral Reviews*, 2024.

Houthooft, R., Chen, X., Duan, Y., Schulman, J., De Turck, F., and Abbeel, P. VIME: Variational information maximizing exploration. In *Advances in Neural Information Processing Systems*, 2016.

Ionescu-Tulcea, C. Mesures dans les espaces produits. *Atti della Accademia Nazionale dei Lincei. Rendiconti*, 1949.

Jiang, N., Kulesza, A., and Singh, S. Abstraction selection in model-based reinforcement learning. In *International Conference on Machine Learning*, 2015.

Keramati, R., Dann, C., Tamkin, A., and Brunskill, E. Being optimistic to be conservative: Quickly learning a CVaR policy. In *Proceedings of the AAAI Conference on Artificial Intelligence*, 2020.

Kim, M. J., Pertsch, K., Karamcheti, S., Xiao, T., Balakrishna, A., Nair, S., Rafailov, R., Foster, E. P., Sanketi, P. R., Vuong, Q., Kollar, T., Burchfiel, B., Tedrake, R., Sadigh, D., Levine, S., Liang, P., and Finn, C. OpenVLA: An open-source vision-language-action model. In *8th Annual Conference on Robot Learning*, 2024.

Koenker, R. and Bassett Jr, G. Regression quantiles. *Econometrica: journal of the Econometric Society*, 1978.

Krauth, K., Tu, S., and Recht, B. Finite-time analysis of approximate policy iteration for the linear quadratic regulator. In *Advances in Neural Information Processing Systems*, 2019.

Kuznetsov, A., Shvechikov, P., Grishin, A., and Vetrov, D. Controlling overestimation bias with truncated mixture of continuous distributional quantile critics. In *International Conference on Machine Learning*, 2020.

Lanillos, P., Meo, C., Pezzato, C., Meera, A. A., Baioumy, M., Ohata, W., Tschantz, A., Millidge, B., Wisse, M., Buckley, C. L., et al. Active inference in robotics and artificial agents: Survey and challenges. *arXiv preprint arXiv:2112.01871*, 2021.

Lazaric, A. and Restelli, M. Transfer from multiple MDPs. In *Advances in Neural Information Processing Systems*, 2011.

Li, L., Walsh, T., and Littman, M. Towards a unified theory of state abstraction for MDPs. In *International Symposium on Artificial Intelligence and Mathematics*, 2006.

Li, S., Pang, Y., Bai, P., Li, J., Liu, Z., Hu, S., Wang, L., and Wang, G. Learning locomotion for quadruped robots via distributional ensemble actor-critic. *IEEE Robotics and Automation Letters*, 2024.

Lim, S. H. and Malik, I. Distributional reinforcement learning for risk-sensitive policies. In *Advances in Neural Information Processing Systems*, 2022.

Ma, X., Chen, J., Xia, L., Yang, J., Zhao, Q., and Zhou, Z. Dsac: Distributional soft actor-critic for risk-sensitive reinforcement learning. *Journal of Artificial Intelligence Research*, 2025.

Malekzadeh, P. and Plataniotis, K. N. Active inference and reinforcement learning: A unified inference on continuous state and action spaces under partial observability. *Neural Computation*, 2024.

Marković, D., Stojić, H., Schwöbel, S., and Kiebel, S. J. An empirical evaluation of active inference in multi-armed bandits. *Neural Networks*, 2021.

Mavrin, B., Yao, H., Kong, L., Wu, K., and Yu, Y. Distributional reinforcement learning for efficient exploration. In *International Conference on Machine Learning*, 2019.

Mazzaglia, P., Verbelen, T., and Dhoedt, B. Contrastive active inference. In *Advances in Neural Information Processing Systems*, 2021.

Millidge, B. Deep active inference as variational policy gradients. *Journal of Mathematical Psychology*, 2020.

Millidge, B. *Applications of the Free Energy Principle to Machine Learning and Neuroscience*. PhD thesis, University of Edinburgh, 2021.

Millidge, B., Tschantz, A., Seth, A. K., and Buckley, C. L. On the relationship between active inference and control as inference. In *International Workshop on Affective Interactions*, 2020.

Nam, D. W., Kim, Y., and Park, C. Y. GMAC: A distributional perspective on actor-critic framework. In *International Conference on Machine Learning*, 2021.

NVIDIA Research, Bjorck, J., Castañeda, F., Cherniadev, N., Da, X., Ding, R., Fan, L. J., Fang, Y., Fox, D., Hu, F., Huang, S., Jang, J., Jiang, Z., Kautz, J., Kundalia, K., Lao, L., Li, Z., Lin, Z., Lin, K., Liu, G., Llontop, E., Magne, L., Mandlekar, A., Narayan, A., Nasiriany, S., Reed, S., Tan, Y. L., Wang, G., Wang, Z., Wang, J., Wang, Q., Xiang, J., Xie, Y., Xu, Y., Xu, Z., Ye, S., Yu, Z., Zhang, A., Zhang, H., Zhao, Y., Zheng, R., and Zhu, Y. Gr0ot n1: An open foundation model for generalist humanoid robots. *arXiv preprint arXiv:2503.14734*, 2025.

Oh, J., Kim, J., and Yun, S.-Y. Risk perspective exploration in distributional reinforcement learning. In *ICML 2022 Workshop AI for Agent-Based Modelling*, 2022.

Osband, I., Russo, D., and Van Roy, B. (more) efficient reinforcement learning via posterior sampling. In *Advances in Neural Information Processing Systems*, 2013.

Ostrovski, G., Bellemare, M. G., van den Oord, A., and Munos, R. Count-based exploration with neural density models. In *International Conference on Machine Learning*, 2017.

Parr, T., Pezzulo, G., and Friston, K. J. *Active Inference: The Free Energy Principle in Mind, Brain, and Behavior*. The MIT Press, 2022.

Pathak, D., Agrawal, P., Efros, A. A., and Darrell, T. Curiosity-driven exploration by self-supervised prediction. In *International Conference on Machine Learning*, 2017.

Paul, A., Sajid, N., Gopalkrishnan, M., and Razi, A. Active inference for stochastic control. In *Joint European Conference on Machine Learning and Knowledge Discovery in Databases*, 2021.

Pearl, J. Causal diagrams for empirical research. *Biometrika*, 1995.

Rao, R. P. and Ballard, D. H. Predictive coding in the visual cortex: a functional interpretation of some extra-classical receptive-field effects. *Nature neuroscience*, 1999.

Sajid, N., Ball, P. J., and Friston, K. J. Active inference: Demystified and compared. *Neural Computation*, 2021a.

Sajid, N., Tigas, P., Zakharov, A., Fountas, Z., and Friston, K. Exploration and preference satisfaction trade-off in reward-free learning. *arXiv preprint arXiv:2106.04316*, 2021b.

Schneider, L., Frey, J., Miki, T., and Hutter, M. Learning risk-aware quadrupedal locomotion using distributional reinforcement learning. In *International Conference on Robotics and Automation*, 2024.

Schneider, T., Belousov, B., Abdulsamad, H., and Peters, J. Active inference for robotic manipulation. *arXiv preprint arXiv:2206.10313*, 2022.

Shi, J., Bai, C., He, H., Han, L., Wang, D., Zhao, B., Zhao, M., Li, X., and Li, X. Robust quadrupedal locomotion via risk-averse policy learning. In *International Conference on Robotics and Automation*, 2024.

Singh, R., Lee, K., and Chen, Y. Sample-based distributional policy gradient. In *Learning for Dynamics and Control Conference*, 2022.

Sukhija, B., Coros, S., Krause, A., Abbeel, P., and Sferrazza, C. MaxInfoRL: Boosting exploration in reinforcement learning through information gain maximization. In *International Conference on Learning Representations*, 2025.

Sun, K., Zhao, Y., Shi, E., Wang, Y., Yan, X., Jiang, B., and Kong, L. Intrinsic benefits of categorical distributional loss: Uncertainty-aware regularized exploration in reinforcement learning. In *Advances in Neural Information Processing Systems*, 2025.

Tang, Y. and Agrawal, S. Exploration by distributional reinforcement learning. In *International Joint Conference on Artificial Intelligence*, 2018.

Tassa, Y., Doron, Y., Muldal, A., Erez, T., Li, Y., Casas, D. d. L., Budden, D., Abdolmaleki, A., Merel, J., Lefrancq, A., et al. DeepMind control suite. *arXiv preprint arXiv:1801.00690*, 2018.

Tiapkin, D., Belomestny, D., Calandriello, D., Moulines, E., Munos, R., Naumov, A., Rowland, M., Valko, M., and Ménard, P. Optimistic posterior sampling for reinforcement learning with few samples and tight guarantees. In *Advances in Neural Information Processing Systems*, 2022.

Todorov, E., Erez, T., and Tassa, Y. MuJoCo: A physics engine for model-based control. In *IEEE/RSJ International Conference on Intelligent Robots and Systems*, 2012.

Tolstikhin, I., Bousquet, O., Gelly, S., and Schoelkopf, B. Wasserstein auto-encoders. In *International Conference on Learning Representations*, 2018.

Tschantz, A., Baltieri, M., Seth, A. K., and Buckley, C. L. Scaling active inference. In *International Joint Conference on Neural Networks (IJCNN)*, 2020a.

Tschantz, A., Millidge, B., Seth, A. K., and Buckley, C. L. Reinforcement learning through active inference. *arXiv preprint arXiv:2002.12636*, 2020b.

Ueltzhöffer, K. Deep active inference. *Biological Cybernetics*, 2018.

van der Himst, O. and Lanillos, P. Deep active inference for partially observable MDPs. In *International Workshop on Active Inference*, 2020.

Yang, D., Zhao, L., Lin, Z., Qin, T., Bian, J., and Liu, T. Fully parameterized quantile function for distributional reinforcement learning. In *Advances in Neural Information Processing Systems*, 2019.

Yang, K., Tao, J., Lyu, J., and Li, X. Exploration and anti-exploration with distributional random network distillation. In *International Conference on Machine Learning*, 2024.

Yarats, D., Fergus, R., Lazaric, A., and Pinto, L. Mastering visual continuous control: Improved data-augmented reinforcement learning. In *International Conference on Learning Representations*, 2022.

Yu, K. and Moyeed, R. A. Bayesian quantile regression. *Statistics & Probability Letters*, 2001.

Zhang, Y., Corcodel, R., and Zhao, D. Bipedalism for quadrupedal robots: Versatile loco-manipulation through risk-adaptive reinforcement learning. In *International Conference on Humanoid Robots (Humanoids)*, 2025.

Zhou, F., Zhu, Z., Kuang, Q., and Zhang, L. Non-decreasing quantile function network with efficient exploration for distributional reinforcement learning. In *International Joint Conference on Artificial Intelligence*, 2021.

Appendix

Table 2. Notation used throughout the paper.

\triangleq	Definition of a variable.
$:=$	Assignment of an already defined variable to a new value.
$(g \circ h)(x) \triangleq g(h(x))$	Composition of functions g and h for some input x .
$g^{-1}(B) \triangleq \{x \in \mathcal{X} : g(x) \in B\}$	Pre-image of set B under function g .
$\ g(x)\ _\infty \triangleq \sup_{x \in \mathcal{X}} g(x) $	Supremum norm.
$\mathbf{1}(\rho)$	Indicator function; returns 1 if predicate ρ is true, 0 otherwise.
$\text{sign}(x)$	Sign function that returns +1 if $x \geq 0$ and -1 otherwise.
\mathbb{N}	The set of natural numbers $\{0, 1, 2, \dots\}$.
\mathbb{N}_+	The set of strictly positive natural numbers $\{1, 2, 3, \dots\}$.
\mathbb{R}	The set of real numbers.
\mathbb{R}_+	The set of positive real numbers.
$\sigma(\mathcal{X})$	The σ -algebra generated by \mathcal{X} .
$\mathcal{B}(\mathbb{R})$	Borel σ -algebra on \mathbb{R} .
$(\mathcal{X}, \sigma(\mathcal{X}))$	Measurable space with σ -algebra $\sigma(\mathcal{X})$.
$(\mathcal{X}, \sigma(\mathcal{X}), P)$	Probability space constructed by measuring $(\mathcal{X}, \sigma(\mathcal{X}))$ with P .
$\mathcal{P}_{\mathcal{X}}$	The set of all probability measures on $(\mathcal{X}, \sigma(\mathcal{X}))$.
$\delta_x(A) \triangleq \mathbf{1}(x \in A)$	Dirac measure evaluated at x for some measurable set A .
$F_P(x) \triangleq P(X \leq x)$	Cumulative Distribution Function (CDF) of measure P .
$f_P(x) \triangleq dF_P(x)/dx$	Probability Density Function (PDF) of measure P .
$\mathbb{E}_{x \sim P}[g(x)] \triangleq \int_{\mathcal{X}} g(x)P(dx)$	Expected value of measurable function g with respect to probability measure P .
$\mathbb{V}_{x \sim P}[g(x)] \triangleq \int_{\mathcal{X}} g^2(x)P(dx) - (\int_{\mathcal{X}} g(x)P(dx))^2$	Variance of measurable function g with respect to probability measure P .
$P_{X Y}P_{Y z} \triangleq \int P_{X Y}(\cdot Y)P_{Y Z}(dY z) = P_{X z}$	Marginalization of an intermediate random variable Y conditioned on a point observation z .
$P_X P_Y z \triangleq \int P_X(\cdot Y)P_{Y Z}(dY z) = P_{X z}$	Shorthand where the conditioning on Y .
$P_X P_Y \triangleq \int P_X(\cdot Y)P_Y(dY)$	Shorthand for unconditional marginalization.
$\mathcal{U}(a, b)$	Continuous uniform distribution defined on range $a < b \in \mathbb{R}$.
$\mathcal{U}(A)$	Discrete distribution where each element of set A gets equal probability, i.e., $P(X = a) = 1/ A , \forall a \in A$.
$\mathcal{IG}(\sigma \alpha, \beta) = \frac{\beta^\alpha}{\Gamma(\alpha)} \sigma^{-\alpha-1} \exp(-\beta/\sigma)$	Inverse Gamma distribution with shape α and scale β .
Dirichlet(α)	Dirichlet distribution with concentration parameters $\alpha = (\alpha_1, \dots, \alpha_K)$, $\alpha_i > 0$.
$\Gamma(x)$	Gamma function, the continuous extension of the factorial with $\Gamma(n) = (n-1)!$ for positive integers.
$\psi(x)$	Digamma function, the logarithmic derivative of the gamma function: $\psi(x) = \frac{d}{dx} \log \Gamma(x)$.
$\mathbb{H}[P] \triangleq -\int_{\mathcal{X}} \log p(x)P(dx)$	(Differential) entropy.
$KL(P \parallel \bar{P}) \triangleq \int_{\mathcal{X}} \log \left(\frac{dP}{d\bar{P}} \right) P(dx)$	Kullback-Leibler divergence between probability measures P and \bar{P} .
$\Gamma(P, \bar{P})$	The set of couplings between probability measures P and \bar{P} .
$\mathcal{W}_p(P, \bar{P}) \triangleq \left(\inf_{\nu \in \Gamma(P, \bar{P})} \mathbb{E}_{(x, x') \sim \nu} [x - x' ^p] \right)^{1/p}$	p -Wasserstein distance for absolute norm.
$\bar{\mathcal{W}}_p(P_{x,a}, \bar{P}_{x,a}) \triangleq \sup_{x,a} \mathcal{W}_p(P_{x,a}, \bar{P}_{x,a})$	Maximal form of p -Wasserstein distance.
$P_{W \text{do}(X \sim P(\cdot))}$	do-operator that replaces the distribution of variable X in a structural causal model W by P .

A. Proofs and derivations

A.1. Proof of Theorem 3.1

For a fixed (x, a) the Wasserstein distance is regular, homogeneous, and p -convex (see, e.g., Bellemare et al., 2023, Definition 4.22-4.24 for details), i.e.,

$$\begin{aligned} \mathcal{W}_p^p \left(\mathbf{T}_{P_*}^\pi \mathbf{F} \# \mathbb{P}_{x,a}^{P_\pi}, \mathbf{T}_{P_*}^\pi \mathbf{F} \# \mathbb{P}_{x,a}^{\bar{P}_\pi} \right) &\leq \gamma^p \mathcal{W}_p \left(\mathbb{E}_{x' \sim P_\pi^*(x'|x, \pi(x))} \left[\mathbf{F} \# \mathbb{P}_{x', \pi(x)}^{P_\pi} \right], \mathbb{E}_{x' \sim P_\pi^*(x'|x, \pi(x))} \left[\mathbf{F} \# \mathbb{P}_{x', \pi(x)}^{\bar{P}_\pi} \right] \right) \\ &\leq \gamma^p \mathbb{E}_{x' \sim P_\pi^*(x'|x, \pi(x))} \left[\mathcal{W}_p \left(\mathbf{F} \# \mathbb{P}_{x', \pi(x)}^{P_\pi}, \mathbf{F} \# \mathbb{P}_{x', \pi(x)}^{\bar{P}_\pi} \right) \right] \\ &\leq \gamma^p \sup_{x', a'} \mathcal{W}_p^p \left(\mathbf{F} \# \mathbb{P}_{x', \pi(x)}^{P_\pi}, \mathbf{F} \# \mathbb{P}_{x', \pi(x)}^{\bar{P}_\pi} \right) = \gamma^p \bar{\mathcal{W}}_p^p \left(\mathbf{F} \# \mathbb{P}_\pi^{P_\pi}, \mathbf{F} \# \mathbb{P}_\pi^{\bar{P}_\pi} \right), \end{aligned}$$

where the first inequality follows, via regularity and homogeneity, the second via p -convexity, the third via the definition of a supremum and finally the equality via the definition of $\bar{\mathcal{W}}_p$. As this holds for every pair (x, a) taking the p -th root and subsequently the supremum on the left hand side gives the desired inequality \square

A.2. Proof of Lemma 3.4

By definition, $(KF)(x, \cdot) = K(F(x), \cdot)$. Using the L -Lipschitz property of the kernel K on \mathcal{S} , we have:

$$\mathcal{W}_p(K(F(x), \cdot), K(F(x'), \cdot)) \leq L \cdot |F(x) - F(x')|.$$

Applying the M -Lipschitz property of F , it follows that $|F(x) - F(x')| \leq M \cdot |x - x'|$. Substituting this into the inequality above gives:

$$\mathcal{W}_p((KF)(x, \cdot), (KF)(x', \cdot)) \leq L \cdot M \cdot |x - x'| \quad \square$$

A.3. Proof of Theorem 3.5

We apply a cascade of the following two simple results. The first is that passing a Markov kernel through an L -Lipschitz operator is a contraction with respect to p -Wasserstein distance.

Lemma A.1. *For every $P, P' \in \mathcal{P}_{\mathcal{X}}$ and L -Lipschitz Markov kernel K , the following holds:*

$$\mathcal{W}_p(KP, KP') \leq L \cdot \mathcal{W}_p(P, P').$$

Proof. Let π be an optimal coupling for (P, P') with respect to d_p . For every pair $(s, s') \sim \pi$ let $\gamma_{s,s'}$ be the optimal coupling of $(K(s, \cdot), K(s', \cdot))$. We then have

$$\begin{aligned} \mathcal{W}_p^p(KP, KP') &\leq \mathbb{E}_{(s, s') \sim \pi} [\mathcal{W}_p^p(K(s, \cdot), K(s', \cdot))] \\ &\leq \mathbb{E}_{(s, s') \sim \pi} [L \cdot |s - s'|^p] \\ &= L \cdot \mathbb{E}_{(s, s') \sim \pi} [|s - s'|^p] \\ &= L \cdot \mathcal{W}_p^p(P, P'). \end{aligned}$$

The first inequality follows via the definition of the Wasserstein distance as the infimum over all couplings, where the right hand side is the expected distance for the chosen coupling strategy (pairing via π , then $\gamma_{s,s'}$). The second inequality follows via the Lipschitz assumption and the final via the choice of π as the optimal coupling of (P, P') . Taking the p -th root gives the desired inequality. \square

The second is that passing the Markov kernels of two Markov processes through an L -Lipschitz operator contracts their p -Wasserstein distance by a factor L .

Lemma A.2. *Let $\mathbb{P}_{x,a}^P$ and $\mathbb{P}_{x,a}^{P'}$ be the laws of two Markov processes generated by kernels P and P' respectively. Let K be an L -Lipschitz probabilistic operator. Define the transformed processes $\mathbb{P}_{x,a}^{KP}$ and $\mathbb{P}_{x,a}^{KP'}$ as the laws generated by the composed kernels KP and KP' . Then we have*

$$\mathcal{W}_p(\mathbb{P}_{x,a}^{KP}, \mathbb{P}_{x,a}^{KP'}) \leq L \cdot \mathcal{W}_p(\mathbb{P}_{x,a}^P, \mathbb{P}_{x,a}^{P'}).$$

Proof. Let ν be an optimal coupling of the path measures $(\mathbb{P}_{x,a}^P, \mathbb{P}_{x,a}^{P'})$ such that the total cost satisfies $\mathbb{E}_\nu[\sum_{t=0}^\infty |X_t - X'_t|^p] = \mathcal{W}_p^p(\mathbb{P}_{x,a}^P, \mathbb{P}_{x,a}^{P'})$. By the definition of the Wasserstein distance on the product space and the L -Lipschitz property of K , we have for each time step t :

$$\mathcal{W}_p^p(K(X_t, \cdot), K(X'_t, \cdot)) \leq L^p \cdot |X_t - X'_t|^p.$$

Summing over the horizon and taking the limit $T \rightarrow \infty$, we bound the distance between the transformed processes by integrating the point-wise kernel distances over the path coupling ν :

$$\begin{aligned} \mathcal{W}_p^p(\mathbb{P}_{x,a}^{KP}, \mathbb{P}_{x,a}^{KP'}) &\leq \lim_{T \rightarrow \infty} \mathbb{E}_\nu \left[\sum_{t=0}^T \mathcal{W}_p^p(K(X_t, \cdot), K(X'_t, \cdot)) \right] \\ &\leq \lim_{T \rightarrow \infty} \mathbb{E}_\nu \left[\sum_{t=0}^T L^p \cdot |X_t - X'_t|^p \right] \\ &= L^p \cdot \mathbb{E}_\nu \left[\sum_{t=0}^\infty |X_t - X'_t|^p \right] \\ &= L^p \cdot \mathcal{W}_p^p(\mathbb{P}_{x,a}^P, \mathbb{P}_{x,a}^{P'}). \end{aligned}$$

Taking the p -th root yields the desired result. \square

Proof of Theorem 3.5. First, we observe that the transition kernel $(P_D S) : \mathcal{X} \rightarrow \mathcal{P}_{\mathcal{X}}$ is a composition of an L_E -Lipschitz map S and an L_D -Lipschitz kernel P_D . Consequently, $(P_D S)$ is an $(L_D L_E)$ -Lipschitz Markov kernel in the p -Wasserstein sense.

Applying Lemma A.2, the distance between the path-space measures generated by the transformed kernels is bounded by:

$$\mathcal{W}_p \left(\mathbb{P}^{(P_D S)P_\pi}, \mathbb{P}^{(P_D S)\bar{P}_\pi} \right) \leq (L_D L_E) \cdot \mathcal{W}_p \left(\mathbb{P}^{P_\pi}, \mathbb{P}^{\bar{P}_\pi} \right).$$

By the property of the process-level push-forward functional $\mathbf{F}_\#$, this relationship is preserved. Finally, applying the γ -contraction property of the operator $\mathbf{T}_{P_*}^\pi$, we obtain:

$$\begin{aligned} \bar{\mathcal{W}}_p \left(\mathbf{T}_{P_*}^\pi \mathbf{F}_\# \mathbb{P}^{(P_D S)P_\pi}, \mathbf{T}_{P_*}^\pi \mathbf{F}_\# \mathbb{P}^{(P_D S)\bar{P}_\pi} \right) \\ \leq \gamma \cdot \bar{\mathcal{W}}_p \left(\mathbf{F}_\# \mathbb{P}^{(P_D S)P_\pi}, \mathbf{F}_\# \mathbb{P}^{(P_D S)\bar{P}_\pi} \right) \\ \leq \gamma \cdot L_E \cdot L_D \cdot \bar{\mathcal{W}}_p \left(\mathbf{F}_\# \mathbb{P}^{P_\pi}, \mathbf{F}_\# \mathbb{P}^{\bar{P}_\pi} \right). \end{aligned}$$

The result follows. \square

A.4. Factorization of the intervened world model

Define

$$\tilde{P}(X, Y, S) \triangleq P_D(X|Y, S)P_Q(Y, S). \quad (8)$$

Then by product rule

$$\begin{aligned} \tilde{P}(X, Y, S)_{\text{do}(X \sim P_R)} &= \tilde{P}(X|Y, S)_{\text{do}(X \sim P_R)} \tilde{P}(Y, S)_{\text{do}(X \sim P_R)} \\ &= \tilde{P}(X|Y, S)_{\text{do}(X \sim P_R)} \tilde{P}(Y, S) \\ &= P_R(X) \tilde{P}(Y, S) \end{aligned}$$

By definition we have

$$\tilde{P}(X, Y, S)_{\text{do}(X \sim P_R)} = (P_D)_{\text{do}(X \sim P_R)}(X|Y, S)(P_Q)_{\text{do}(X \sim P_R)}(Y, S)$$

$$= P_R(X)P_Q(Y, S).$$

which yields $\tilde{P}(Y, S) = P_Q(Y, S)$ hence

$$\tilde{P}(X, Y, S)_{\text{do}(X \sim P_R)} = P_R(X)P_Q(Y, S).$$

Therefore

$$\tilde{P}(Y, S|X)_{\text{do}(X \sim P_R)} = P_Q(Y, S).$$

A.5. Derivation of the active inference objective

Consider that

$$\begin{aligned} P_{\tilde{W}|\text{do}(Y \sim \delta_y, S \sim P_Q)}(X, Y, S) &= P_{\tilde{W}|\text{do}(Y \sim \delta_y)}(X, Y, S) \\ &= (P_Q(Y, S)P_R(X))_{\text{do}(Y \sim \delta_y)} \\ &= (P_Q(Y, S))_{\text{do}(Y \sim \delta_y)}P_R(X) \\ &= P_Q(y, S)P_R(X). \end{aligned}$$

The first equality follows from the fact that $P_{\tilde{W}}$ has already been constructed with the intervention $\text{do}(S \sim P_Q)$ and the second is due to the result shown in Section A.4. Now the related AIF posterior can be constructed as follows

$$\begin{aligned} \log f_{P_0}(Y := y) + \text{const} &= \mathbb{E}_{x', s \sim P_{W|\text{do}(Y \sim \delta_y, S \sim P_Q)}} \left[L(x', P_{\tilde{W}|\text{do}(Y \sim \delta_y)}, P_Q) \right] \\ &= \mathbb{E}_{x', s \sim P_{W|\text{do}(Y \sim \delta_y, S \sim P_Q)}} \left[\mathbb{E}_{y', s' \sim P_Q} \left[\log \left(P_Q(y, s')P_R(x')/P_Q(y', s') \right) \right] \right] \\ &= \mathbb{E}_{x', s \sim P_{W|\text{do}(Y \sim \delta_y, S \sim P_Q)}} \left[\log P_R(x') + \mathbb{E}_{y', s' \sim P_Q} \left[\log \left(P_Q(y, s')/P_Q(y', s') \right) \right] \right] \\ &= \mathbb{E}_{x' \sim P_D P_{Q|y}} \left[\log P_R(x') \right] + \mathbb{E}_{x' \sim P_D P_{Q|y}} \left[\mathbb{E}_{y', s' \sim P_Q} [\log P_Q(y, s')] - \mathbb{E}_{y', s' \sim P_Q} [\log P_Q(y', s')] \right] \end{aligned}$$

where const represents the normalization constant that does not depend on Y . Now let us take the expectation with respect to the posterior on Y :

$$\begin{aligned} \mathbb{E}_{y \sim P_Q} [\log f_{P_0}(Y := y)] + \text{const} &= \mathbb{E}_{y \sim P_Q} \left[\mathbb{E}_{x' \sim P_D P_{Q|y}} \left[\log P_R(x') \right] + \mathbb{E}_{x' \sim P_D P_{Q|y}} \left[\mathbb{E}_{y', s' \sim P_Q} [\log P_Q(y, s')] - \mathbb{E}_{y', s' \sim P_Q} [\log P_Q(s', y')] \right] \right] \\ &= \mathbb{E}_{x' \sim P_D P_Q} [\log P_R(x')] + \mathbb{E}_{y \sim P_Q} \left[\mathbb{E}_{x' \sim P_D P_{Q|y}} \left[\mathbb{E}_{y', s' \sim P_Q} [\log P_Q(y, s')] - \mathbb{E}_{y', s' \sim P_Q} [\log P_Q(y', s')] \right] \right] \\ &= \mathbb{E}_{x' \sim P_D P_Q} [\log P_R(x')] + \mathbb{E}_{y \sim P_Q} \left[\mathbb{E}_{x' \sim P_D P_{Q|y}} \left[\mathbb{E}_{y', s' \sim P_Q} [\log P_Q(y, s')] \right] \right] - \mathbb{E}_{y \sim P_Q} \left[\mathbb{E}_{y', s' \sim P_Q} [\log P_Q(y', s')] \right] \\ &= \mathbb{E}_{x' \sim P_D P_Q} [\log P_R(x')] + \mathbb{E}_{y \sim P_Q} \left[\mathbb{E}_{x' \sim P_D P_{Q|y}} \left[\mathbb{E}_{y', s' \sim P_Q} [\log P_Q(y, s')] \right] \right] - \mathbb{E}_{y', s' \sim P_Q} [\log P_Q(y', s')] \\ &= \mathbb{E}_{x' \sim P_D P_Q} [\log P_R(x')] + \mathbb{E}_{x', y \sim P_D P_Q} \left[\mathbb{E}_{y', s' \sim P_Q} [\log P_Q(y, s')] \right] - \mathbb{E}_{y', s' \sim P_Q} [\log P_Q(y', s')] \\ &= \mathbb{E}_{x' \sim P_D P_Q} [\log P_R(x')] + \mathbb{E}_{x', y' \sim P_D P_Q} \left[\mathbb{E}_{y, s' \sim P_Q} [\log P_Q(y, s')] \right] - \mathbb{E}_{y', s' \sim P_Q} [\log P_Q(y', s')] \\ &= \mathbb{E}_{x' \sim P_D P_Q} [\log P_R(x')] + \mathbb{E}_{y, s' \sim P_Q} [\log P_Q(y, s')] - \mathbb{E}_{y', s' \sim P_Q} [\log P_Q(y', s')] \\ &= \mathbb{E}_{x' \sim P_D P_Q} [\log P_R(x')]. \end{aligned}$$

Plugging this result into the ELBO, we get

$$L(x, P_W, P_Q) = \mathbb{E}_{y, s \sim P_Q} \left[\log \left(P_D(x|y, s)P_0(y, s)/P_Q(y, s) \right) \right]$$

$$\begin{aligned}
 &= \mathbb{E}_{y,s \sim P_Q} [\log P_D(x|y,s)] + \mathbb{E}_{y,s \sim P_Q} [\log P_0(y,s)] + \mathbb{H}[P_Q] \\
 &= \mathbb{E}_{y,s \sim P_Q} [\log P_D(x|y,s)] + \mathbb{E}_{y,s \sim P_Q} [\log P_0(s|y)] + \mathbb{E}_{y \sim P_Q} [\log P_0(y)] + \mathbb{H}[P_Q] \\
 &= \mathbb{E}_{y,s \sim P_Q} [\log P_D(x|y,s)] + \mathbb{E}_{y,s \sim P_Q} [\log P_0(s|y)] + \mathbb{E}_{x' \sim P_D P_Q} [\log P_R(x')] + \mathbb{H}[P_Q].
 \end{aligned}$$

A.6. Derivation of the upper bound to the push-forward RL objective

$$\begin{aligned}
 J(S) &= \mathbb{E}_{x \sim \mathcal{U}(\mathcal{X})} [d_2^2((\mathbf{G}_{x_0, a_0}^\pi)_{\#} \mathbb{P}_{x_0, a_0}^{(P_D S) P_\pi}, \mathbf{T}_{P_*}^\pi (\mathbf{G}_{x', \pi(x')}^\pi)_{\#} \mathbb{P}_{x_0, a_0}^{(P_D S) P_\pi})] \\
 &\leq \mathbb{E}_{x \sim \mathcal{U}(\mathcal{X})} [\mathbb{E}_{\mathbf{s} \sim \mathbf{S}_{\#} \mathbb{P}_{x_0, a_0}^{P_\pi}} [d_2^2((\mathbf{G}_{x_0, a_0}^\pi)_{\#} \mathbb{P}_{x_0, a_0}^{P_D | \mathbf{s}}(B), \mathbf{T}_{P_*}^\pi \mathbf{G}_{x', \pi(x')}^\pi)_{\#} \mathbb{P}_{x_0, a_0}^{P_D | \mathbf{s}}(B))] \\
 &= \mathbb{E}_{x \sim \mathcal{U}(\mathcal{X})} \left[\mathbb{E}_{\mathbf{s} \sim \mathbf{S}_{\#} \mathbb{P}_{x_0, a_0}^{P_\pi}} \left[\int_0^1 \left(F_{(\mathbf{G}_{x_0, a_0}^\pi)_{\#} \mathbb{P}_{x_0, a_0}^{P_D | \mathbf{s}}}^{-1}(\tau) - F_{\mathbf{T}_{P_*}^\pi \mathbf{G}_{x', \pi(x')}^\pi)_{\#} \mathbb{P}_{x_0, a_0}^{P_D | \mathbf{s}}}^{-1}(\tau) \right)^2 d\tau \right] \right] \\
 &= \mathbb{E}_{x \sim \mathcal{U}(\mathcal{X})} \left[\mathbb{E}_{\mathbf{s} \sim \mathbf{S}_{\#} \mathbb{P}_{x_0, a_0}^{P_\pi}} \left[\mathbb{E}_{\tau \in \mathcal{U}(0,1)} \left[\left(\left(F_{(\mathbf{G}_{x_0, a_0}^\pi)_{\#} \mathbb{P}_{x_0, a_0}^{P_D | \mathbf{s}}}^{-1}(\tau) - F_{\mathbf{T}_{P_*}^\pi \mathbf{G}_{x', \pi(x')}^\pi)_{\#} \mathbb{P}_{x_0, a_0}^{P_D | \mathbf{s}}}^{-1}(\tau) \right)^2 \right] \right] \right]
 \end{aligned}$$

where the inequality follows from the composite nature of $(\mathbf{G}_{x_0, a_0}^\pi)_{\#} \mathbb{P}_{x_0, a_0}^{(P_D S) P_\pi}$ established in Eq. 5. The result follows straightforwardly from the role of couplings in the p -Wasserstein distance formulation and it is commonly used by prior work in other contexts such as Wasserstein Auto Encoders (Tolstikhin et al., 2018).

B. Experiment Details

B.1. Tabular environments

B.1.1. RIVERSWIM

The RiverSwim (Osband et al., 2013) environment is defined over a one-dimensional state space $\mathcal{X} = \{1, \dots, n\}$ with binary actions $\mathcal{A} = \{-1, +1\}$. The transition dynamics are parameterized by probabilities p_{forward} and p_{backward} and are given by

$$\begin{aligned}
 P(X' = k+1 | X = k, A = +1) &= p_{\text{forward}} \mathbf{1}(2 \leq k \leq n-1) + (1 - (p_{\text{forward}} + p_{\text{backward}})) \mathbf{1}(k = 1), \\
 P(X' = k | X = k, A = +1) &= (1 - (p_{\text{forward}} + p_{\text{backward}})) \mathbf{1}(k \geq 2) + (p_{\text{forward}} + p_{\text{backward}}) \mathbf{1}(k = 1), \\
 P(X' = k-1 | X = k, A = +1) &= p_{\text{backward}} \mathbf{1}(2 \leq k \leq n-1) + (p_{\text{forward}} + p_{\text{backward}}) \mathbf{1}(k = n), \\
 P(X' = k+1 | X = k, A = -1) &= 0, \\
 P(X' = k | X = k, A = -1) &= \mathbf{1}(k = 1), \\
 P(X' = k-1 | X = k, A = -1) &= \mathbf{1}(k-1 \geq 1).
 \end{aligned}$$

The desired state distribution (reward) is given by

$$P_R(X = n) = 0.99, \quad P_R(X = 1) = 0.005, \quad P_R(X \notin \{1, n\}) = \frac{0.005}{n-2}.$$

B.1.2. LATENT RIVERSWIM

We introduce the Latent RiverSwim environment that extends RiverSwim to a two-dimensional observation space

$$\mathcal{X} = \{1, \dots, n\}^2,$$

with action space

$$\mathcal{A} = \{(+1, 0), (-1, 0), (0, +1), (0, -1)\},$$

and a one-dimensional latent state space

$$\mathcal{S} = \{1, \dots, n\},$$

which defines the latent manifold. The latent encoding and transition dynamics are defined as

$$e_\alpha(i, j) = \alpha i + (1 - \alpha)j, \quad (i, j) \in \mathcal{X} \quad (\text{state encoder}),$$

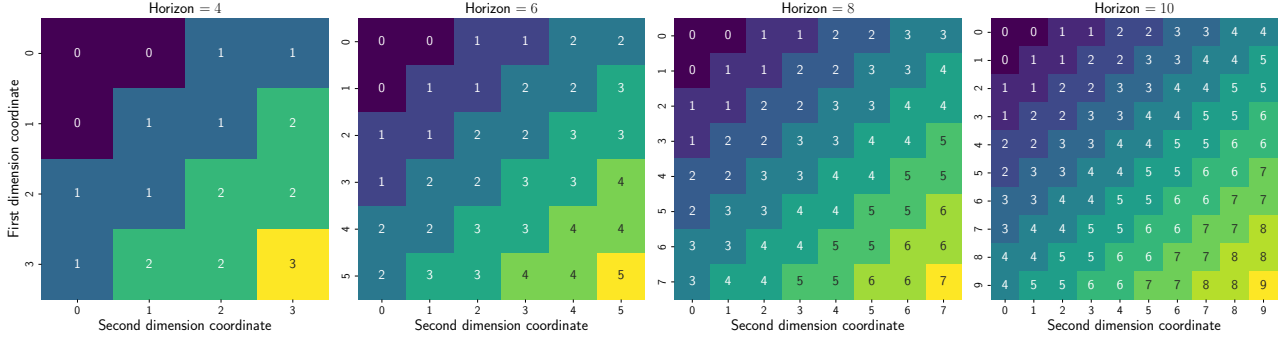


Figure 3. Observation-to-latent state mappings in the Latent RiverSwim environment across multiple horizons. The (i, j) coordinates represent indices for each observation in \mathcal{X} , while cell values and colours indicate the corresponding latent state index from \mathcal{S} . For instance, at Horizon = 4, the cell $(i = 3, j = 1)$ has value 2, signifying that observation $(3, 1)$ is mapped to latent state 2 by the encoding process. This visualization demonstrates that when the transitions and rewards originate from a lower-dimensional manifold, the encoder naturally forms equivalence classes among observations through state abstraction. This abstraction reduces the complexity of the mapping, inducing a more favourable Lipschitz constant for the decoder.

Algorithm 4 Tabular PSRL-PI

Input: $\pi(\cdot) := \mathcal{U}(\mathcal{A})$, $\gamma \in (0, 1)$, Dirichlet concentration parameter $\alpha_{x,a} : \mathcal{X} \times \mathcal{A} \rightarrow \mathbb{R}_+^{|\mathcal{X}|}$, $\gamma \in (0, 1)$

while True **do**

- $a = \pi(x)$
- $x', r := \text{env.step}(a)$
- $\alpha_{x,a}(x') := \alpha_{x,a}(x') + 1$
- $\hat{P}_\alpha(\cdot|x, a) \sim \text{Dirichlet}(\alpha_{x,a}(\cdot)) \quad \forall x, a$
- repeat**
- $V_\pi = \left(I - \gamma \hat{P}_\alpha(x, \pi(x), \cdot) \right)^{-1} P_R$
- $\pi(x) := \arg \max_a P_R(x) + \gamma \sum_{x'} \hat{P}_\alpha(x'|x, a) V_\pi(x') \quad \forall x \in \mathcal{X}$
- until** policy π is stable
- end while**

$$k = \lfloor e_\alpha(i, j) \rfloor \quad (\text{latent state}),$$

$$\bar{a} = \text{sign}(e_\alpha(a_1, a_2)), \quad (a_1, a_2) \in \mathcal{A} \quad (\text{latent action}),$$

for $\alpha \in (0, 1)$. The latent transition and reward dynamics follow those of RiverSwim with the identification $S \triangleq \mathcal{X}$. The decoder maps a latent state k back to the observation space by uniformly sampling one of the states consistent with the encoding:

$$P_D(X|S = k) = \mathcal{U}(\{X : \lfloor e_\alpha(i, j) \rfloor = k, (i, j) \in \mathcal{X}\}). \quad (9)$$

B.1.3. TABULAR ALGORITHMS

We present the state of the art in tabular model-based reinforcement learning using a policy-iteration variant of posterior sampling for reinforcement learning (PSRL-PI), summarized in Algorithm 4. As a representative of state-of-the-art distributional reinforcement learning in the tabular setting, we consider Algorithm 5, which captures the key properties of implicit quantile networks. Our distributional active inference method can be implemented in tabular or discrete-action settings by extending the IQQL algorithm in Algorithm 5. We refer to the resulting method as *Distributional Active Inference (DAIF)*, which is presented in Algorithm 6. For details, see Section B.2.4.

B.1.4. EXPERIMENTS

We evaluate the tabular methods described above on the RiverSwim and Latent RiverSwim environments using 50 independent repetitions. For RiverSwim, the agents interact with the environment for 5000 steps, while for Latent RiverSwim they

Algorithm 5 Tabular Implicit Quantile Q Learning (IQQL)

Input: $Q_\tau(\cdot, \cdot) := 0, \pi(\cdot) := \mathcal{U}(\mathcal{A}), D := \emptyset, \gamma \in (0, 1)$

while True **do**

$a := \pi(x)$

$x', r := \text{env.step}(a)$

$D := D \cup (x, a, r, x')$

repeat

$(\tilde{x}, \tilde{a}, \tilde{r}, \tilde{x}') \sim D, \quad \tau, \tau' \sim \mathcal{U}(0, 1)$

$Q_\tau(\tilde{x}, \tilde{a}) := \arg \min_{Q'_\tau} \ell_\tau(\tilde{r} + \gamma Q_{\tau'}(\tilde{x}', \pi(\tilde{x}')) - Q'_\tau(\tilde{x}, \tilde{a}))$

$\ell_\tau(u) \triangleq \frac{|u| + (2\tau - 1)u}{2}$

until end of training epoch

$\pi(x) := \arg \max_{a'} \mathbb{E}_{\tau'' \sim \mathcal{U}(0, 1)} [Q_{\tau''}(x, a')] \quad \forall x \in X$

end while

Algorithm 6 Tabular Distributional Active Inference (DAIF)

Input: $Q_\tau(\cdot, \cdot) := 0, \pi(\cdot) := \mathcal{U}(\mathcal{A}), D := \emptyset, \gamma \in (0, 1)$

while True **do**

$a := \pi(x)$

$x', r := \text{env.step}(a)$

$D := D \cup (x, a, r, x')$

repeat

$(\tilde{x}, \tilde{a}, \tilde{r}, \tilde{x}') \sim D, \quad \tau, \tau' \sim \mathcal{U}(0, 1)$

$\mu, \alpha, \beta := Q_\tau(\tilde{x}, \tilde{a}), \quad \mu' := Q_{\tau'}(\tilde{x}', \pi(\tilde{x}')), \quad G := \tilde{r} + \gamma \mu'$

$Q_\tau(\tilde{x}, \tilde{a}) := \arg \max_{Q_\tau} \left\{ \log \tau(1 - \tau) - \log \beta + \psi(\alpha) - \frac{\alpha}{2\beta} (|G - \mu| + (2\tau - 1)(G - \mu)) \right\}$

until end of training epoch

$\pi(x) := \arg \max_{a'} \mathbb{E}_{\tau'' \sim \mathcal{U}(0, 1)} [Q_{\tau''}(x, a')] \quad \forall x \in X$

end while

interact for 10 000 steps. The first 10% of the interactions are performed using a random policy to initialize exploration. For the IQQL and DAIF models, we use neural networks to approximate the value functions. In RiverSwim, we employ a single linear layer, whereas in Latent RiverSwim we use a multilayer perceptron with ReLU activations and a single hidden layer of width 128. Figure 4 reports the results in terms of the frequency of visiting the most desired state within a 100-step window for varying horizon.

B.2. Continuous control environments

B.2.1. EvoGym

EvoGym (Bhatia et al., 2021) provides continuous control tasks for soft robots with deformable bodies, which introduce non-stationarity into the control dynamics and make the learning problem more challenging. As our focus is on the control optimization problem rather than robot morphology design, we do not design or evolve robot structures. Instead, we adopt the highest-reward robot morphologies provided in the EvoGym repository.² These morphologies were identified by Bhatia et al. (2021) through co-optimization of robot design and control, and represent structures that are well-suited to each task. By using these previously optimized designs, we isolate the control learning problem and ensure a fair comparison across algorithms without confounding effects from morphology variation. From the available environments, we choose seven tasks spanning different difficulty levels and task types to provide a comprehensive evaluation.

Locomotion tasks. We include four locomotion environments: (1) *Walker-v0* (easy), where the objective is to travel as far as possible in a single direction; (2) *UpStepper-v0* (medium), where the robot must climb stairs of varying heights; (3) *BidirectionalWalker-v0* (medium), where the target position changes dynamically during the episode, requiring the agent to learn locomotion in both directions; and (4) *Traverser-v0* (hard), where the robot must cross a pit without sinking.

²<https://huggingface.co/datasets/EvoGym/robots>



Figure 4. Top: RiverSwim. Bottom: Latent RiverSwim. Solid lines indicate the mean over 50 seeds, and shaded regions represent the standard error.

Object manipulation tasks. We include three manipulation environments: (1) *Thrower-v0* (medium), where a box is placed on top of the robot and must be thrown over obstacles of varying sizes; (2) *Catcher-v0* (hard), where the robot must catch a rapidly falling and rotating box dropped from a height; and (3) *Lifter-v0* (hard), where the robot must lift a box out of a hole.

Excluded environments. From the original benchmark set, we exclude *Carrier-v0*, *BridgeWalker-v0*, *Climber-v0*, and *BeamSlider-v0*. We exclude *Carrier-v0* because it is classified as easy, and our evaluation prioritizes more challenging tasks while retaining one easy task as a baseline. We exclude *BridgeWalker-v0*, *Climber-v0*, and *BeamSlider-v0* because preliminary experiments showed minimal performance variance across algorithms in our initial seeds, limiting their discriminative value. Our final choice ensures balanced coverage across difficulty levels (one easy, three medium, three hard) and task types (four locomotion, three manipulation).

Inclusion of non-benchmark environment. We include *BidirectionalWalker-v0*, which is not part of the original benchmark set, because it introduces a qualitatively different locomotion challenge: the agent must learn to move in both directions in response to a dynamically changing goal, testing adaptability beyond standard unidirectional locomotion.

Figure 5 shows the learning curves across EvoGym environments, while Table 3 reports the numerical results in terms of AULC and final return.

B.2.2. DEEPMIND CONTROL SUITE

DeepMind Control Suite (DMC) (Tassa et al., 2018) provides a diverse set of continuous control tasks built on the MuJoCo physics engine (Todorov et al., 2012) and is widely used as a benchmark for reinforcement learning algorithms. From the available environments, we choose eight tasks that span different robot morphologies and difficulty levels.

Dog tasks. The *dog* robot has the largest state and action space dimensionality in DMC. We include *dog-walk*, *dog-trot*, and *dog-run* to evaluate performance across increasing difficulty on this challenging morphology.

Run tasks across robots. We include *cheetah-run*, *walker-run*, *quadruped-run*, and *humanoid-run*. These robots range from planar (*cheetah*, *walker*) to 3D (*quadruped*, *humanoid*) and vary in state dimensionality and control complexity. We choose the *run* task as it is the most demanding locomotion variant for each robot.

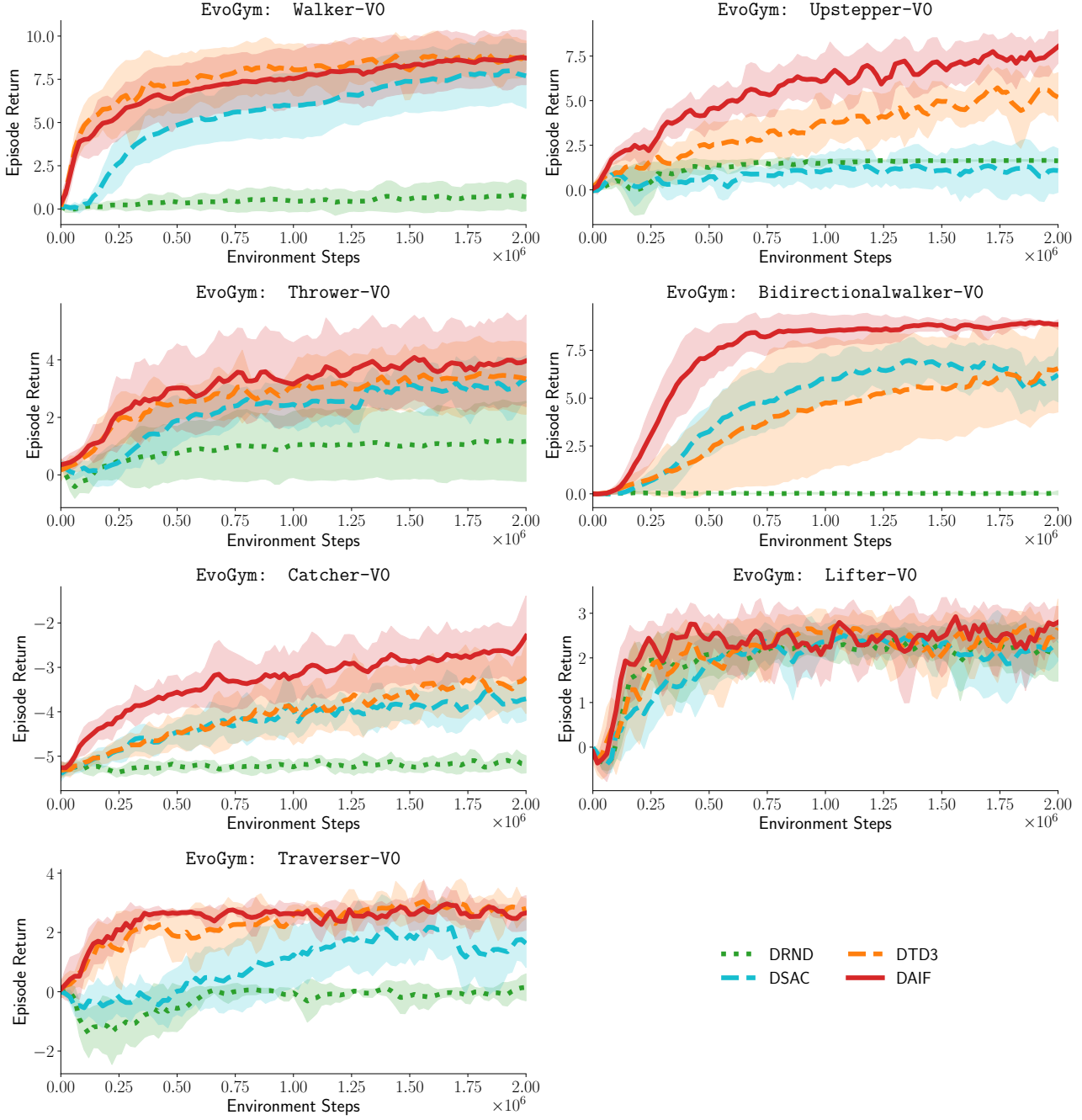


Figure 5. Learning curves for EvoGym environments.

Figure 6 presents the learning curves across DMC environments, while Table 4 reports the corresponding numerical results in terms of AULC and final return.

B.2.3. DMC VISION.

The environments and tasks are identical to those in the state-based DMC setting; however, the agent learns directly from pixel observations rather than proprioceptive state inputs. Following the experimental setup of Yarats et al. (2022), we adopt their task difficulty categorization and hyperparameter configurations.

We evaluate on five tasks: *cheetah-run*, *quadruped-run*, *walker-run*, *reacher-hard*, and *finger-turn-hard*. The three *run* tasks

Table 3. Area Under the Learning Curve (AULC) and Final Return (mean \pm standard deviation) averaged over 10 repetitions on the EvoGym environments. The highest mean values are highlighted in bold, and results within one standard deviation distance to the highest mean performance are underlined.

Metric	Environment	Model			
		DRND	DSAC	DTD3	DAIF
AULC (\uparrow)	Walker-V0	0.47 ± 0.54	5.54 ± 1.32	7.60 ± 1.24	<u>7.16 ± 1.47</u>
	Upstepper-V0	1.33 ± 0.17	0.88 ± 0.60	3.44 ± 0.92	5.56 ± 0.77
	Thrower-V0	0.86 ± 0.99	<u>2.19 ± 0.48</u>	<u>2.71 ± 0.71</u>	3.12 ± 1.17
	Bidirectionalwalker-V0	0.02 ± 0.01	4.68 ± 0.86	3.94 ± 2.09	7.21 ± 0.55
	Catcher-V0	-5.21 ± 0.06	-4.22 ± 0.23	-4.06 ± 0.41	<u>-3.31 ± 0.39</u>
	Lifter-V0	1.98 ± 0.26	1.88 ± 0.29	2.11 ± 0.28	2.27 ± 0.23
FINAL RETURN (\uparrow)	Traverser-V0	-0.26 ± 0.18	0.92 ± 0.53	2.30 ± 0.25	2.43 ± 0.14
	Walker-V0	0.63 ± 0.75	7.78 ± 1.74	8.91 ± 0.86	<u>8.80 ± 1.55</u>
	Upstepper-V0	1.62 ± 0.06	0.97 ± 1.28	5.08 ± 2.07	8.35 ± 0.78
	Thrower-V0	1.17 ± 1.40	<u>3.34 ± 0.80</u>	<u>3.38 ± 1.17</u>	4.08 ± 1.64
	Bidirectionalwalker-V0	0.06 ± 0.15	6.11 ± 1.89	6.78 ± 2.41	8.79 ± 0.37
	Catcher-V0	-5.23 ± 0.20	-3.58 ± 0.39	-3.27 ± 0.93	<u>-2.22 ± 1.01</u>
	Lifter-V0	2.21 ± 0.72	<u>2.34 ± 0.41</u>	2.70 ± 1.06	2.74 ± 0.51
	Traverser-V0	0.16 ± 0.49	1.54 ± 1.14	2.85 ± 0.31	<u>2.62 ± 0.90</u>

Table 4. Area Under the Learning Curve (AULC) and Final Return (mean \pm standard deviation) averaged over 10 repetitions on the DeepMind Control suite environments. The highest mean values are highlighted in bold, and results within one standard deviation distance to the highest mean performance are underlined.

Metric	Environment	Model			
		DRND	DSAC	DTD3	DAIF
AULC (\uparrow)	Dog-Walk	53.28 ± 74.94	468.31 ± 69.04	503.09 ± 53.94	575.84 ± 50.52
	Dog-Trot	22.12 ± 30.23	189.95 ± 51.30	<u>313.05 ± 28.88</u>	368.90 ± 78.55
	Dog-Run	17.92 ± 21.89	97.20 ± 19.02	162.40 ± 15.52	214.37 ± 31.33
	Cheetah-Run	666.37 ± 30.09	548.75 ± 38.19	540.36 ± 60.55	646.65 ± 56.03
	Humanoid-Run	22.02 ± 26.71	12.06 ± 15.63	66.22 ± 35.79	<u>61.56 ± 20.06</u>
	Quadruped-Run	605.52 ± 101.59	658.64 ± 39.26	<u>681.68 ± 28.00</u>	720.89 ± 47.59
FINAL RETURN (\uparrow)	Walker-Run	<u>615.66 ± 28.31</u>	<u>637.58 ± 31.87</u>	546.43 ± 69.38	638.04 ± 88.82
	Dog-Walk	171.67 ± 256.17	887.32 ± 21.58	887.64 ± 17.45	910.25 ± 20.23
	Dog-Trot	53.55 ± 88.03	514.18 ± 121.13	612.97 ± 112.84	736.52 ± 117.58
	Dog-Run	19.39 ± 31.78	184.70 ± 19.24	260.35 ± 35.76	382.27 ± 56.21
	Cheetah-Run	819.29 ± 58.72	700.53 ± 39.77	685.59 ± 61.70	<u>815.95 ± 52.73</u>
	Humanoid-Run	51.92 ± 62.32	42.14 ± 51.26	<u>115.84 ± 57.97</u>	138.56 ± 25.29
	Quadruped-Run	809.23 ± 81.57	809.65 ± 60.31	835.89 ± 46.84	873.91 ± 17.54
	Walker-Run	736.29 ± 29.58	736.46 ± 38.15	636.76 ± 81.69	<u>730.13 ± 106.01</u>

test locomotion from pixels across different morphologies, while *reacher-hard* and *finger-turn-hard* provide non-locomotion tasks requiring precise control. We exclude *dog* tasks because Yarats et al. (2022) did not evaluate on this environment and no reference configurations are available. We also exclude *humanoid-run*, which is categorized as hard and requires 30 000 000 frames, 10 \times increase over the medium-difficulty tasks we consider.

We use DrQ-v2 as the backbone for our implementation, adopting DDPG-style exploration. The DTD3 variant corresponds to the distributional extension of DrQ-v2. We use the learning curves provided in the official repository³. Figure 7 presents the learning curves across DMC Vision environments, while Table 5 reports the corresponding numerical results in terms of

³<https://github.com/facebookresearch/drqv2>

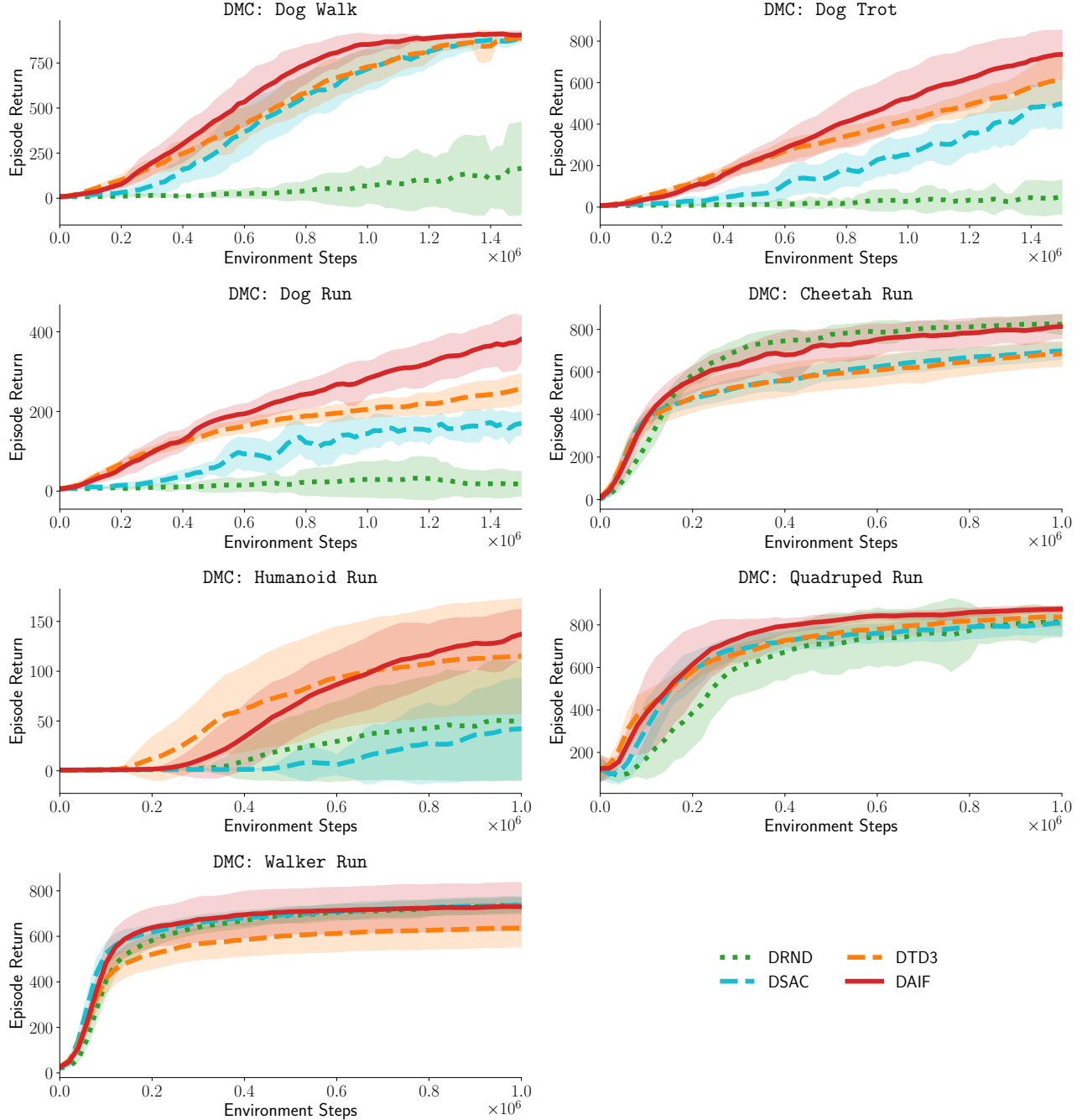


Figure 6. Learning curves for DeepMind Control suite environments.

AULC and final return.

B.2.4. IMPLEMENTATION DETAILS

Given an observation tuple (x, a, τ) , we define the input-dependent hyperpriors

$$\mu \triangleq \mu_\phi(x, a, \tau), \quad \alpha \triangleq \alpha_\phi(x, a, \tau), \quad \beta \triangleq \beta_\phi(x, a, \tau),$$

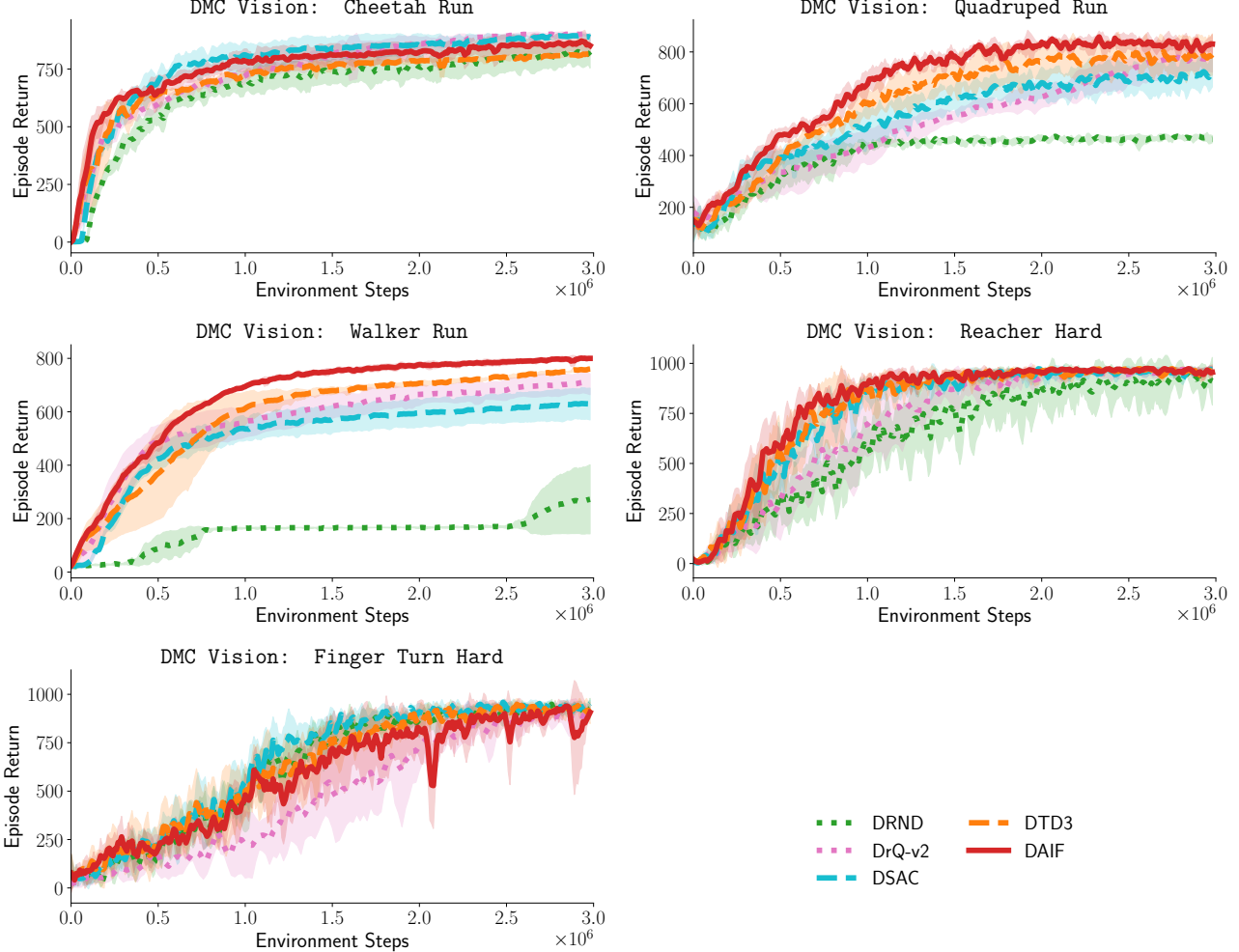


Figure 7. Learning curves for DeepMind Control suite vision environments.

 Table 5. Area Under the Learning Curve (AULC) and Final Return (mean \pm standard deviation) averaged over 5 repetitions on the DeepMind Control suite vision environments. The highest mean values are highlighted in bold, and results within one standard deviation distance to the highest mean performance are underlined.

Metric	Environment	Model				
		DRND	DrQ-v2	DSAC	DTD3	DAIF
AULC (\uparrow)	Cheetah-Run	663.13 \pm 38.98	<u>743.02</u> \pm 9.45	770.48 \pm 33.96	707.78 \pm 17.05	<u>756.45</u> \pm 32.60
	Quadruped-Run	402.28 \pm 10.70	526.64 \pm 27.79	550.19 \pm 41.06	613.70 \pm 44.27	676.43 \pm 18.12
	Walker-Run	149.66 \pm 10.64	565.91 \pm 39.92	509.54 \pm 42.86	587.99 \pm 41.96	659.73 \pm 6.49
	Reacher-Hard	640.13 \pm 96.90	706.24 \pm 59.81	773.13 \pm 12.60	<u>783.05</u> \pm 44.43	807.19 \pm 27.02
	Finger-Turn Hard	<u>627.22</u> \pm 23.88	481.89 \pm 82.63	661.09 \pm 35.50	627.93 \pm 59.60	580.21 \pm 57.50
FINAL RETURN (\uparrow)	Cheetah-Run	800.57 \pm 61.43	894.25 \pm 8.88	880.97 \pm 24.16	814.80 \pm 8.87	859.80 \pm 55.21
	Quadruped-Run	474.37 \pm 8.94	761.76 \pm 51.41	733.71 \pm 55.48	<u>796.24</u> \pm 71.23	832.98 \pm 54.93
	Walker-Run	273.97 \pm 130.92	699.36 \pm 39.57	628.40 \pm 59.10	761.66 \pm 5.90	802.47 \pm 5.40
	Reacher-Hard	903.28 \pm 132.70	<u>969.82</u> \pm 5.22	970.62 \pm 13.02	954.34 \pm 36.76	954.84 \pm 36.89
	Finger-Turn Hard	918.26 \pm 85.21	941.10 \pm 35.56	965.00 \pm 4.97	882.76 \pm 92.06	920.58 \pm 48.30

where μ_ϕ , α_ϕ , and β_ϕ are outputs of a neural network parameterized by ϕ . We denote $\mathbf{m} \triangleq (\mu, \alpha, \beta)$. The corresponding generative model is defined as

$$\sigma \sim \mathcal{IG}(\alpha, \beta), \quad G|\mu, \sigma, \tau \sim \mathcal{ALD}(\mu, \sigma, \tau),$$

where \mathcal{ALD} denotes the asymmetric Laplace distribution with density

$$f(G|\mu, \sigma, \tau) = \frac{\tau(1-\tau)}{\sigma} \exp\left(-\ell_\tau\left(\frac{G-\mu}{\sigma}\right)\right),$$

and the check function is defined as $\ell_\tau(u) = \frac{|u| + (2\tau - 1)u}{2}$. The corresponding log-likelihood is given by

$$\log f(G|\mu, \sigma, \tau) = \log \tau(1-\tau) - \log \sigma - \frac{|G-\mu| + (2\tau-1)(G-\mu)}{2\sigma}.$$

Rather than drawing reparameterized samples from the inverse-gamma distribution, we analytically marginalize over σ . Taking the expectation of the log-likelihood with respect to the inverse-gamma prior yields

$$\begin{aligned} \mathbb{E}_\sigma[\log f(G|\mu, \sigma, \tau)] &= \log \tau(1-\tau) - \mathbb{E}_\sigma[\log \sigma] \\ &\quad - \frac{1}{2} (|G-\mu| + (2\tau-1)(G-\mu)) \mathbb{E}_\sigma\left[\frac{1}{\sigma}\right]. \end{aligned}$$

We first compute $\mathbb{E}_\sigma[\log \sigma]$. For $\sigma \sim \mathcal{IG}(\alpha, \beta)$,

$$\mathbb{E}_\sigma[\log \sigma] = \int_0^\infty \log \sigma \frac{\beta^\alpha}{\Gamma(\alpha)} \sigma^{-(\alpha+1)} \exp\left(-\frac{\beta}{\sigma}\right) d\sigma.$$

Applying the change of variables $a = \beta/\sigma$ yields

$$\begin{aligned} \mathbb{E}_\sigma[\log \sigma] &= \frac{1}{\Gamma(\alpha)} \int_0^\infty (\log \beta - \log a) a^{\alpha-1} \exp(-a) da \\ &= \log \beta - \psi(\alpha), \end{aligned}$$

where $\psi(\cdot)$ denotes the digamma function. Next, we compute $\mathbb{E}_\sigma[1/\sigma]$. Using the same change of variables,

$$\mathbb{E}_\sigma\left[\frac{1}{\sigma}\right] = \frac{\beta^\alpha}{\Gamma(\alpha)} \int_0^\infty \sigma^{-(\alpha+2)} \exp\left(-\frac{\beta}{\sigma}\right) d\sigma = \frac{\alpha}{\beta},$$

where we used the identity $\Gamma(\alpha+1) = \alpha\Gamma(\alpha)$. Combining the above results, we obtain

$$\mathbb{E}_\sigma[\log f(G|\mu, \sigma, \tau)] = \log \tau(1-\tau) - \log \beta + \psi(\alpha) - \frac{\alpha}{2\beta} (|G-\mu| + (2\tau-1)(G-\mu)). \quad (10)$$

We use the negative of this expected log-likelihood as the critic training objective. To mitigate numerical instabilities, we enforce α and β to be larger than 10 by adding a constant offset of 10 to the corresponding network outputs. In addition, we adopt the regularization strategy proposed by [Akgül et al. \(2025\)](#) who placed weak hyperpriors

$$p(\mu) = \mathcal{N}(0, 1000^2), \quad p(\alpha) = \mathcal{G}(10, 0.1), \quad p(\beta) = \mathcal{G}(10, 0.1),$$

where the priors over α and β are defined over the shifted parameters. We use this regularization with a regularization coefficient $\xi = 0.001$.

We adopt the design choices of [Ma et al. \(2025\)](#) combined with action-noise exploration and delayed policy updates ([Fujimoto et al., 2018](#)). The full update procedure is presented in Algorithm 7. The algorithm proceeds as follows: first, quantiles are randomly sampled and their midpoints are computed. Next, the target action is obtained from the lagged target actor with clipped Gaussian noise added. The parameters of the asymmetric Laplace distribution, μ and σ are estimated for the current state-action pair and quantiles, where we model $\sigma \sim \mathcal{IG}(\alpha, \beta)$. Temporal difference errors are then computed for each critic using min-clipping. The critic loss is the negative log-likelihood weighted by pairwise quantile regression weights following [Ma et al. \(2025\)](#); [Yang et al. \(2019\)](#); specifically, line 23 weights each TD error by $(\tau_{i+1} - \tau_i)$, which corresponds to the quantile bin width and ensures that each quantile contributes proportionally to its probability mass under the target distribution. Regularization terms are computed using the priors, followed by parameter and Polyak updates for the critics. Every d^{th} step (where $d = 2$), the policy is updated: quantiles and midpoints are recomputed, an action is sampled from the online actor, and the actor maximizes the estimated mean μ over the quantile distribution, followed by parameter and Polyak updates. For DMC vision control environments, we also apply the random augmentation method of [Yarats et al. \(2022\)](#) to our baselines.

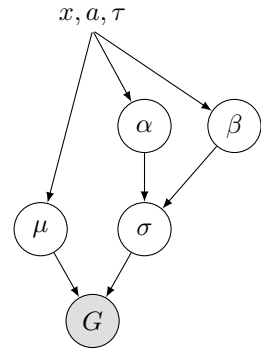


Figure 8. The plate diagram of the deep actor-critic implementation of DAIF. Each circle indicates a random variable. The observed random variable G is shaded and the other ones are latent.

Algorithm 7 Distributional Active Inference update

1: **Parameters:** N : number of quantiles, γ : discount factor, ι : Polyak averaging parameter, π_σ : policy exploration noise scale, π_c : policy noise clip bound, d : policy update delay interval, and ξ : regularization coefficient
 2: **Networks:** π_θ : policy network with parameters θ , $\mu_{\phi_k}, \alpha_{\phi_k}, \beta_{\phi_k}$: critic networks ($k = 1, 2$) with parameters ϕ_k , and $\bar{\phi}_k$: target network parameters
 3: **Input:** Transition (x, a, r, x') from replay buffer
 4: — *Critic Update* —
 5: Sample and sort $\{\tau_i\}_{i=0}^N, \{\tau_j\}_{j=0}^N \sim \mathcal{U}(0, 1)$; compute midpoints $\hat{\tau}_i, \hat{\tau}_j$
 6: $a' := \pi_{\bar{\theta}}(x') + \text{clip}(\epsilon, -\pi_c, \pi_c)$ where $\epsilon \sim \mathcal{N}(0, \pi_\sigma^2 I)$ \triangleright *action-noise exploration*
 7: Compute $\mu_j^k, \alpha_j^k, \beta_j^k$ from critic networks for $k \in \{1, 2\}, j \in \{0, \dots, N-1\}$
 8: Compute TD errors: $u_{ij}^k := r + \gamma \min_{k'} \mu_{\bar{\phi}_{k'}}(x', a', \hat{\tau}_i) - \mu_j^k$ for all i, j, k \triangleright *Min-clipping*
 9: — *Critic Loss (via Equation (10))* —
 10: **for** $k = 1, 2$ **do**
 11: $\mathcal{L}(\phi_k) := -\frac{1}{N} \sum_{i,j} (\tau_{i+1} - \tau_i) \left[\log \hat{\tau}_j (1 - \hat{\tau}_j) - \log \beta_j^k + \psi(\alpha_j^k) - \frac{\alpha_j^k}{2\beta_j^k} (|u_{ij}^k| + (2\hat{\tau}_j - 1)u_{ij}^k) \right]$
 12: $\mathcal{L}(\phi_k) := \mathcal{L}(\phi_k) - \xi \frac{1}{N} \sum_j (\log p(\mu_j^k) + \log p(\alpha_j^k) + \log p(\beta_j^k))$
 13: **end for**
 14: Update ϕ_k via $\nabla_{\phi_k} \mathcal{L}(\phi_k)$; $\bar{\phi}_k := \iota \phi_k + (1 - \iota) \bar{\phi}_k$ for $k = 1, 2$ \triangleright *SGD + Polyak*
 15: — *Policy Update* —
 16: **if** $t \bmod d = 0$ **then**
 17: Sample and sort $\{\tau_i\}_{i=0}^N \sim \mathcal{U}(0, 1)$; compute midpoints $\hat{\tau}_i$
 18: $\mathcal{L}(\theta) := -\frac{1}{2} \sum_{k,i} (\tau_{i+1} - \tau_i) \mu_{\phi_k}(x, \pi_\theta(x), \hat{\tau}_i)$
 19: Update θ via $\nabla_\theta \mathcal{L}(\theta)$; $\bar{\theta} := \iota \theta + (1 - \iota) \bar{\theta}$ \triangleright *SGD + Polyak*
 20: **end if**

B.2.5. TRAINING

Baselines. We include DRND (Yang et al., 2024) as a representative exploration-driven model-free reinforcement learning baseline. We also consider DSAC (Ma et al., 2025), the most recent state-of-the-art distributional actor–critic algorithm for continuous control. In addition, we introduce DTD3, a distributional extension of TD3 (Fujimoto et al., 2018), to directly assess whether DAIF improves over a distributional variant of TD3. For the DMC vision experiments, we include DrQ-v2 (Yarats et al., 2022), which achieves the highest reported scores among model-free methods on DMC vision environments. While model-based approaches such as DreamerV3 (Hafner et al., 2025) achieve strong performance, they require learning a world model, which is orthogonal to our focus on model-free policy optimization. Notably, at 1 000 000 environment steps (2 000 000 frames), DAIF achieves competitive or superior performance compared to DreamerV3 on several tasks: DAIF outperforms DreamerV3 on *quadruped-run* (813 vs. 617), *walker-run* (780 vs. 684), and *reacher-hard* (950 vs. 862), while achieving comparable performance on *cheetah-run* (823 vs. 836) and *finger-turn-hard* (867 vs. 904). This demonstrates that our model-free approach can match or exceed the performance of state-of-the-art model-based methods without the additional complexity of world model learning.

Critic architecture. We adopt the critic architecture of Ma et al. (2025) for continuous control tasks, except for DMC Vision environments. The critic takes the state, action, and quantile fraction as inputs and outputs the parameters (μ, α, β) . The architecture follows a modular design with separate embeddings for the state–action pair and the quantile fraction, which are fused to produce the final quantile value estimates. Specifically, the state–action input is processed by a base network consisting of a linear layer with 256 hidden units, followed by layer normalization and a ReLU activation. The quantile fraction τ is embedded using a separate quantile network that maps a 128-dimensional quantile encoding to a 256-dimensional representation via a linear layer, layer normalization, and a sigmoid activation. The resulting embeddings are combined through element-wise interaction and passed to an output network comprising an additional hidden layer with 256 units, layer normalization, and ReLU activation, followed by a final linear layer that outputs scalar values for μ , α , and β .

For DMC Vision control tasks, in addition to the critic architecture described above, we employ the convolutional encoder of [Yarats et al. \(2022\)](#) to process high-dimensional observations. The encoder consists of four convolutional layers with 32 channels each. The first layer uses a stride of 2, while the remaining layers use stride 1. Each convolution is followed by a ReLU activation, and the resulting feature maps are flattened to obtain a compact latent representation. After the encoder, we use a Linear layer that maps the output of the encoder to a feature dimension of 50, followed by layer normalization and tanh activation for both actor and critic.

Actor architecture. We parametrize the actor by a multilayer perceptron that maps the state representation to a continuous action. The network consists of two hidden layers with 256 units each, each followed by a ReLU activation. A final linear layer outputs the action vector, which is subsequently passed through a tanh activation to enforce bounded actions within the valid action range. This architecture provides sufficient expressive capacity for modeling complex continuous policies while remaining computationally efficient and stable in practice. For DMC Vision control tasks, the same actor architecture is used on top of the encoder, and a DDPG-style exploration scheme is applied following [Yarats et al. \(2022\)](#).

Optimization. We use a learning rate of 3×10^{-4} for both the actor and the critic, except for DMC Vision control tasks, where a learning rate of 1×10^{-4} is used for the actor, critic, and encoder. We employ a replay buffer of size 1 000 000 and a batch size of 256, with 10 000 environment steps for warm-up. The discount factor is set to 0.99, and Polyak averaging with a coefficient of 0.005 is used for target network updates. We use two critics and a single actor, with target networks maintained for both. Policy smoothing is applied using Gaussian noise with standard deviation 0.1, target policy noise with standard deviation 0.2, and target noise clipping of 0.5, together with a policy update delay of 2. We randomly sample 8 quantiles for value estimation, target computation, and actor training. The regularization coefficient is set to $\xi = 0.001$. For DMC Vision tasks, we use a frame stack of 3 and an action repeat of 2, and all other hyperparameters follow [Yarats et al. \(2022\)](#)⁴.

Environment interactions. We interact with the environments for 1 000 000 steps for DMC control tasks, except for dog environments, where we use 1 500 000 interaction steps. For EvoGym environments, we perform 2 000 000 interaction steps, while for DMC Vision tasks we train for 3 000 000 environment frames. All experiments are repeated 10 times, except for DMC Vision tasks, where we use 5 repetitions.

Ablation study on DAIF with SAC. We also investigate the performance of DAIF with SAC version (DAIF-SAC) on three representative environments chosen from each suite. As shown in Table 6, DAIF-SAC performs well across all three environments, consistently outperforming its base algorithm DSAC on Catcher-V0 and Dog-Run, while achieving comparable performance on Quadruped-Run. These results demonstrate that DAIF can be effectively applied to distributional versions of actor-critic algorithms beyond TD3. It is worth noting that in the DMC Vision tasks, DTD3 and DAIF are based on DrQ-v2, which employs DDPG as its backbone, further highlighting the flexibility of our approach across different actor-critic frameworks.

Table 6. Area Under the Learning Curve (AULC) and Final Return (mean \pm standard deviation) averaged over repetitions. The highest mean values are highlighted in bold, and results within one standard deviation of the best are underlined.

Metric	Environment	Model					
		DRND	DrQ-v2	DSAC	DTD3	DAIF	DAIF-SAC
AULC (\uparrow)	Catcher-V0	-5.21 ± 0.06	—	-4.22 ± 0.23	-4.06 ± 0.41	-3.31 ± 0.39	-3.84 ± 0.23
	Dog-Run	17.92 ± 21.89	—	97.20 ± 19.02	162.40 ± 15.52	214.37 ± 31.33	138.08 ± 27.49
	Quadruped-Run	402.28 ± 10.70	526.64 ± 27.79	550.19 ± 41.06	613.70 ± 44.27	676.43 ± 18.12	512.26 ± 78.71
FINAL RETURN (\uparrow)	Catcher-V0	-5.23 ± 0.20	—	-3.58 ± 0.39	-3.27 ± 0.93	-2.22 ± 1.01	-3.53 ± 0.57
	Dog-Run	19.39 ± 31.78	—	184.70 ± 19.24	260.35 ± 35.76	382.27 ± 56.21	299.70 ± 50.61
	Quadruped-Run	474.37 ± 8.94	761.76 ± 51.41	733.71 ± 55.48	796.24 ± 71.23	832.98 ± 54.93	702.88 ± 92.04

Wall-clock time comparison. We measure wall-clock training time for 10 000 environment interaction steps on the Dog-Run task from the DMC suite, using a system equipped with a GeForce RTX 4090 GPU, an Intel Core i7-14700K CPU (5.6 GHz), and 96 GB memory. DTD3 requires 59.69 seconds, DAIF 66.81 seconds, DSAC 75.05 seconds, and DRND

⁴<https://github.com/facebookresearch/drqv2/tree/c0c650b76c6e5d22a7eb5f2edfffd1440fe94f8ef>

81.69 seconds. Relative to its baseline DTD3, DAIF incurs an overhead of approximately 12% in wall-clock time. These results indicate that the performance improvements achieved by DAIF come at only a modest additional computational cost over its underlying actor–critic architecture.

C. Extended Related Works

C.1. Distributional Reinforcement Learning

Distributional RL explicitly models the full return distribution rather than only its expectation. While it was initially introduced for value-based algorithms (Bellemare et al., 2017; Dabney et al., 2018b;a; Yang et al., 2019), subsequent work extended these ideas to actor–critic architectures, particularly in continuous control settings (Barth-Maron et al., 2018). Various distributional actor–critic variants have been proposed to address specific limitations, including training instability arising from categorical critics (Nam et al., 2021; Singh et al., 2022), overestimation bias (Kuznetsov et al., 2020; Li et al., 2024; Döring et al., 2025), and risk-sensitive decision making (Ma et al., 2025), with several approaches focusing on risk-aware locomotion control (Shi et al., 2024; Schneider et al., 2024; Zhang et al., 2025). Our work generalizes the distributional reinforcement learning framework by working with push-forward mappings of trajectory measures, where the new push-forward RL formulation extends the distributional RL. This generalization allows us to integrate the active inference framework into distributional RL, which in turn lets us develop model-free RL algorithms for active inference. The term *push-forward* also appears in Bai et al. (2025), but there it refers to transport-map parameterizations of action/return distributions from base noise, whereas our push-forward RL pushes forward trajectory measures within the Bellman theory. Therefore the overlap is primarily terminological. In our experiments, we compare our method against distributional RL baselines such as the distributional Soft Actor–Critic (DSAC) (Ma et al., 2025) and Implicit Quantile Q-Learning (Dabney et al., 2018a). To our knowledge, our method is the first to integrate active inference into the distributional reinforcement learning framework.

C.2. Directed Exploration in Reinforcement Learning

Directed exploration explicitly guides reinforcement learning agents toward uncertain or informative states, proving essential in non-stationary environments with changing dynamics and sparse-reward settings lacking frequent feedback. While directed exploration has been extensively studied in the context of classical reinforcement learning algorithms (Houthooft et al., 2016; Bellemare et al., 2016; Pathak et al., 2017; Ostrovski et al., 2017; Burda et al., 2019; Ciosek et al., 2019; Yang et al., 2024), distributional reinforcement learning also provides a natural foundation for exploration. In particular, distributional losses have been shown to induce intrinsic exploration through uncertainty-aware regularization (Sun et al., 2025). Beyond this implicit effect, several works explicitly design exploration strategies within the distributional reinforcement learning framework. Tang & Agrawal (2018) exploit epistemic uncertainty in return distributions for posterior sampling-like exploration; Mavrin et al. (2019) introduce Decaying Left Truncated Variance to derive an optimistic bonus from upper-tail quantiles with decaying optimism; Zhou et al. (2021) propose Distributional Prediction Error, using Wasserstein distance between quantile distributions to construct exploration bonuses; Oh et al. (2022) schedule risk levels from risk-seeking to risk-averse to balance exploration; and Cho et al. (2023) randomize risk criteria through distributional perturbations to avoid biased optimism. While these methods explicitly design exploration bonuses, the exploration term in our distributional actor–critic objective arises naturally from variational free-energy minimization. For directed exploration baselines, we also consider DSAC, which has been shown to exhibit intrinsic exploration effects (Sun et al., 2025). In addition, we include DRND (Yang et al., 2024), a recent state-of-the-art exploration method for actor–critic algorithms.

C.3. Active Inference and Reinforcement Learning

Active inference has increasingly been examined in relation to reinforcement learning as an alternative that unifies perception, action, and learning by minimizing expected free energy (EFE) without explicit rewards or value functions (Friston et al., 2009; 2015; Ueltzhöffer, 2018; Sajid et al., 2021a; Çatal et al., 2019; Tschantz et al., 2020b; Fountas et al., 2020; Millidge et al., 2020; Millidge, 2020; Hafner et al., 2020b). A growing body of empirical work shows that active inference can solve standard reinforcement learning benchmarks, often achieving performance comparable to classical reinforcement learning algorithms (Cullen et al., 2018; van der Himst & Lanillos, 2020; Tschantz et al., 2020a; Marković et al., 2021; Paul et al., 2021). Despite these advantages, particularly the intrinsic balancing of goal-seeking and information gain through epistemic value, most practical AIF agents remain *model-based*, relying on learned generative/world models, belief (variational) inference, and often explicit planning or lookahead to evaluate and optimize EFE (Lanillos et al., 2021; Tschantz et al.,

2020a; Fountas et al., 2020; Schneider et al., 2022; Sajid et al., 2021b). This reliance contributes to the computational burden of multi-step EFE estimation and has historically kept many scalable demonstrations either in discrete settings or in continuous-control implementations with relatively short effective planning horizons (Lanillos et al., 2021; Da Costa et al., 2023). Closest in spirit to our work, Malekzadeh & Plataniotis (2024) derive Bellman-style recursions for EFE and instantiate actor-critic updates; however, their formulation operates in belief space and still depends on learned belief representations and a learned world model for objective construction/evaluation, whereas our approach targets the model-free setting.